

DOKUZ EYLÜL UNIVERSITY
GRADUATE SCHOOL OF NATURAL AND APPLIED SCIENCES

**TWO CHANNEL EMG CLASSIFICATION FOR
TRANSRADIAL ARM MOVEMENTS**



by

Ozan UĞUR

January, 2020

İZMİR

TWO CHANNEL EMG CLASSIFICATION FOR TRANSRADIAL ARM MOVEMENTS

A Thesis Submitted to the

Graduate School of Natural and Applied Sciences of Dokuz Eylül University

In Partial Fulfillment of the Requirements for the Degree of Master of Science

in Biomedical Technologies Program

by

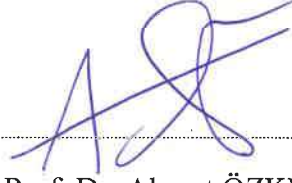
Ozan UĞUR

January, 2020

İZMİR

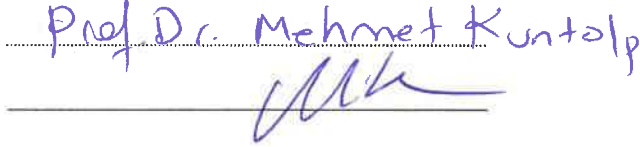
M.Sc THESIS EXAMINATION RESULT FORM

We have read the thesis entitled “**TWO CHANNEL EMG CLASSIFICATION FOR TRANSRADIAL ARM MOVEMENTS**” completed by **OZAN UĞUR** under the supervision of **ASSOC. PROF. DR. AHMET ÖZKURT** and we certify that in our opinion it is fully adequate, in scope and in quality, as a thesis for the degree of Master of Science.

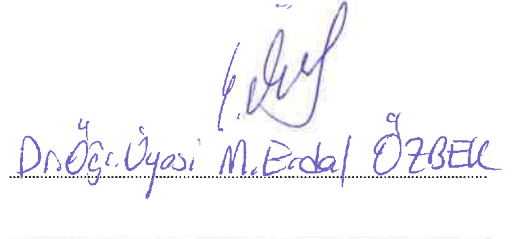


Assoc Prof. Dr. Ahmet ÖZKURT

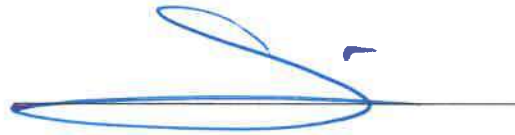
Supervisor



(Jury Member)



(Jury Member)



Prof. Dr. Kadriye ERTEKİN

Director

Graduate School of Natural and Applied Sciences

ACKNOWLEDGMENTS

I would like to express my sincere thanks of gratitude to my supervisor Assoc. Prof. Dr. Ahmet Özkurt who gave me the opportunity to work in this wonderful project. I am also grateful to him for all his assistance during the project. I would like to thank him for giving me the opportunity to work with him during my M.Sc degree and improving my vision during this process.

I would like to thank my colleagues who understood the difficulty of working in the private sector and completing such a challenging M.Sc degree at the same time. Without their support and understanding, this process would be even more challenging.

Finally, and most importantly, I would like to extend special thanks to my mother, Nursen Uğur, for her support and patience. Without her unrequited support and motivation, I would not have been able to complete this thesis. I am grateful to her for her everlasting trust in me.

Ozan UĞUR

TWO CHANNEL EMG CLASSIFICATION FOR TRANSRADIAL ARM MOVEMENTS

ABSTRACT

In this thesis, the classification algorithm for electromyography (EMG) based prosthesis which can be developed for individuals who have undergone transradial arm amputation has been studied using artificial neural networks (ANN). Surface electromyography (sEMG) has been preferred for ease of application in order to receive EMG signals. The data were processed and various features were extracted. Mean absolute value (MAV), root mean square (RMS), simple square integral (SSI), variance of EMG (VAR), log detector (LOG), maximum fractal length (MFL), wavelength (WL), average amplitude change (AAC), difference absolute standard deviation value (DASDV), Willison amplitude (WAMP) and slope sign change (SSC) features are given as an input matrix to the ANN to be trained for classification purposes. In this study, four different movements as relaxed hand, hand close, wrist flexion, and forearm supination are classified.

The accuracy, sensitivity, specificity, and precision performance metrics were calculated as a result of ANN training and examined and interpreted. As a result of the study carried out within the scope of this thesis, the effects of the number of hidden layer neurons, feature extraction, feature selection and individualization of ANN to classification performance were evaluated. A classifier that provides high classification performance metrics were established by training with feature sets formed by grouping and combining features with individual low accuracy rates. The two feature sets created achieved 88 percent accuracy with generalization and 95 percent accuracy with individualization.

Keywords: Transradial arm prosthesis, signal processing, electromyography features, artificial neural networks, pattern recognition

TRANSRADİYAL KOL HAREKETLERİ İÇİN İKİ KANAL EMG SINIFLANDIRMASI

ÖZ

Bu tez kapsamında, transradyal kol amputasyonu geçirmiş bireylere yönelik geliştirilebilecek Elektromiyografi tabanlı bir protez için yapay sinir ağları (YSA) kullanılarak sınıflandırma algoritması üzerine çalışılmıştır. Elektromiyografi (EMG) sinyallerinin alınması için, uygulama kolaylığı göz önünde bulundurularak yüzey electromyografisi tercih edilmiştir. Tek kanal üzerinden alınan verilerin sınıflandırma için yetersiz olması nedeniyle, kaydedilen veriler işlenerek çeşitli özellikler çıkartılmıştır. Ortalama mutlak değer, karekök ortalama, basit kare integrali, EMG varyansı, log detektörü, maksimum fraktal uzunluğu, dalgaboyu, ortalama genlik değişimi, diferansiyel mutlak standart sapma değeri, willison genliği ve eğim işaret değişikliği özellikleri sınıflandırma amacıyla eğitilecek YSA girdi matrisi olarak verilmiştir. Bu çalışmada, açık el, kapalı el, bilek fleksiyonu ve ön kol supinasyonu olmak üzere dört farklı hareket sınıflandırılmıştır.

YSA eğitimleri sonucunda doğruluk, duyarlılık, özgüllük ve kesinlik performans metrikleri hesaplanmış, incelenmiş ve değerlendirilmiştir. Bu tez kapsamında yapılan çalışma sonucunda gizli katman düğümü sayısının, özellik çıkarma, özellik seçimi ve YSA'nın kişiselleştirilmesinin sınıflandırma performansına etkileri değerlendirilmiştir. Bireysel olarak düşük doğruluk oranlarına sahip özelliklerin gruplandırılması ve kombine edilmesi ile oluşturulan özellik kümeleri ile YSA eğitilerek yüksek performans metrikleri sağlayan bir sınıflandırıcı oluşturulmuştur. Oluşturulan iki özellik seti genelleme ile yüzde 88, kişiselleştirme ile yüzde 95 doğruluk elde edilmiştir.

Anahtar kelimeler: Transradyal kol protezi, sinyal işleme, elektromiyografi özellikleri, yapay sinir ağları, örüntü tanıma

CONTENTS

	Page
M.Sc THESIS EXAMINATION RESULT FORM	ii
ACKNOWLEDGMENTS.....	iii
ABSTRACT	iv
ÖZ	v
LIST OF FIGURES	ix
LIST OF TABLES.....	xii
 CHAPTER ONE - INTRODUCTION	 1
 CHAPTER TWO - HUMAN ANATOMY.....	 4
2.1 Anatomical Planes	4
2.2 Muscle Physiology	7
2.2.1 Muscle Types	7
2.3 Skeletal Muscle Structure	7
2.3.1 Forearm Muscles	8
2.4 Transradial Amputation	11
 CHAPTER THREE - DESIGN OF STUDY.....	 13
3.1 EMG Sampling Equipment.....	14
3.2 Signal Acquisition	16
3.3 Signal Processing	18
3.4 Feature Extraction	19

3.4.1 Energy Information.....	23
3.4.1.1 Mean Absolute Value	23
3.4.1.2 Root Mean Square	23
3.4.1.3 Log Detector.....	23
3.4.1.4 Simple Square Integral.....	23
3.4.1.5 Variance of EMG.....	23
3.4.2 Complexity Information.....	23
3.4.2.1 Maximum Fractal Length.....	23
3.4.2.2 Waveform Length.....	24
3.4.2.3 Average Amplitude Change	24
3.4.2.4 Difference Absolute Standard Deviation Value	24
3.4.3 Frequency Information.....	24
3.4.3.1 Willison Amplitude.....	24
3.4.3.2 Slope Sign Change.....	24
3.4.4 MATLAB	24
3.5 Feature Selection	25
 CHAPTER FOUR - RESULTS.....	25
 4.1 Classification.....	40
4.1.1 Feature Set 1	40
4.1.2 Feature Set 2.....	42
4.1.3 Generalized and Individualized Classification.....	45
4.1.1 Effects of Feature Groups on ANN Accuracy	52

CHAPTER FIVE - CONCLUSION	54
--	-----------

REFERENCES	56
-------------------------	-----------



LIST OF FIGURES

	Page
Figure 1.1 Block diagram of the process of the EMG classification system	2
Figure 2.1 Anatomical planes.....	5
Figure 2.2 Illustration of directional terms in human anatomy	6
Figure 2.3 Structure of skeletal muscle.....	8
Figure 2.4 Muscles of the anterior portion of the forearm. A) First layer B) Second layer C) Third layer D) The fourth layer.....	9
Figure 2.5 A healed post transradial amputation patient	11
Figure 2.6 Illustration of transradial amputation.....	12
Figure 3.1 Block diagram of study	13
Figure 3.2 Myoware EMG Sensor.....	15
Figure 3.3 Sensor layout	15
Figure 3.4 Sensor placement blue - innervation zone, green – correct placement, purple – midline offset, orange – myotendon junction.....	16
Figure 3.5 Positioning of EMG electrodes.....	18
Figure 3.6 EMG signals with minimum-maximum normalization	18
Figure 3.7 Amplitudes of raw EMG signal and energy information features for different movements	21
Figure 3.8 Amplitudes of complexity and frequency information features for different movements	22
Figure 3.9 Structure of ANN training with SCG function	27
Figure 3.10 Accuracy rates of ANN training with SCG training function for EI group with variant hidden layer neurons	28
Figure 3.11 Accuracy rates of ANN training with SCG training function for the CI group with variant hidden layer neurons.....	29
Figure 3.12 Accuracy rates of ANN training with SCG training function for FI group with variant hidden layer neurons	29
Figure 3.13 Accuracy rates of ANN training with SCG training function for 40 hidden layer neurons	30
Figure 3.14 Structure of ANN training with LM function.....	30

Figure 3.15 Accuracy rates of ANN training with LM training function for EI group with variant hidden layer neurons	33
Figure 3.16 Accuracy rates of ANN training with LM training function for the CI group with variant hidden layer neurons.....	33
Figure 3.17 Accuracy rates of ANN training with LM training function for FI group with variant hidden layer neurons	34
Figure 3.18 Accuracy rates of ANN training with LM training function for 40 hidden layer neurons	34
Figure 3.19 Structure of ANN training with BR function	35
Figure 3.20 Accuracy rates of ANN training with BR training function for EI group with variant hidden layer neurons	37
Figure 3.21 Accuracy rates of ANN training with BR training function for CI group with variant hidden layer neurons	37
Figure 3.22 Accuracy rates of ANN training with BR training function for FI group with variant hidden layer neurons	38
Figure 3.23 Accuracy rates of ANN training with BR training function for 40 hidden layer neurons	38
Figure 4.1 Structure of ANN training with SCG, LM and BR functions for the feature set 1	40
Figure 4.2 Mean accuracy of ANN with Set 1 and the variant number of hidden layer neurons.	41
Figure 4.3 Structure of ANN training with SCG, LM and BR functions for the feature set 2	43
Figure 4.4 Mean accuracy of ANN with Set 2 and variant number of hidden layer neurons.	43
Figure 4.5 Structure of generalized ANN training with SCG, LM and BR functions for the feature set 1	45
Figure 4.6 Performance plot of generalized ANN training.	45
Figure 4.7 Structure of individualized ANN training with SCG, LM and BR functions for the feature set 1	47
Figure 4.8 Performance plot of individualized ANN training for subject 1.	47
Figure 4.9 Performance plot of individualized ANN training for subject 2.	48

Figure 4.10 Structure of individualized ANN training with LM function for the feature set 1	49
Figure 4.11 Performance plot of trained ANN with the feature set 1.....	49
Figure 4.12 Performance plot of trained ANN with the feature set 2.....	50
Figure 4.13 Structure of individualized ANN training with LM function for raw EMG data	50
Figure 4.14 Structure of individualized ANN training with LM function for the feature set 1 and raw EMG data	51
Figure 4.15 Performance plot of trained ANN with raw EMG data	51
Figure 4.16 Performance plot of trained ANN with raw EMG data and feature set 1	52

LIST OF TABLES

	Page
Table 2.1 Directional terms in human anatomy	6
Table 2.2 Transradial arm muscles and their properties	10
Table 3.1 Feature groups and mathematical representations	20
Table 3.2 MATLAB codes for feature extraction	25
Table 3.3 Performance metrics	26
Table 3.4 Mean accuracy of 10 SCG train trials for EI Group	27
Table 3.5 Mean accuracy of 10 SCG train trials for the CI group and FI Group	28
Table 3.6 Mean accuracy of 10 LM train trials for EI group	31
Table 3.7 Mean accuracy of 10 LM train trials for CI Group and FI Group	32
Table 3.8 Mean accuracy of 10 BR train trials for EI group	35
Table 3.9 Mean accuracy of 10 BR train trials for the CI group and FI group	36
Table 4.1 Sensitivity of ANN training with Set 1	41
Table 4.2 Specificity of ANN training with Set 1	42
Table 4.3 Precision of ANN training with Set 1	42
Table 4.4 Sensitivity of ANN training with Set 2	44
Table 4.5 Specificity of ANN training with Set 2	44
Table 4.6 Precision of ANN training with Set 2	44
Table 4.7 Accuracy rates of generalized ANN	46
Table 4.8 Accuracy rate of individually trained ANNs.	48
Table 4.9 Accuracy rate of trained ANNs with external data.	49
Table 4.10 Effects of feature groups on ANN accuracy	52
Table 4.11 Effect of feature exclusion on ANN accuracy.	53

CHAPTER ONE

INTRODUCTION

Human hand functions are essential for many daily activities such as dressing up, eating, drinking water or opening a door. (Micera, Carpaneto, & Raspopovic, 2010). Individuals who suffer upper limb extremity due to amputation, experience serious psychological and functional problems (Farina & Aszmann, 2014). The occurrence rate of upper extremity amputations is relatively higher in young individuals (Kung et al., 2013).

A prosthetic limb might help the amputee to be capable to do daily activities. In the past decades, researches on upper limb prostheses have grown significantly (Iqbal, Subramaniam, & Shaniba Asmi, 2018). Although primitive prostheses such as the wooden leg or hook hand used in the past have been replaced by prostheses that provide high performance and freedom of movement, the purpose of prostheses has not changed (Oweis, Rihani, & Alkhawaja, 2014). Prostheses require more complex actuators to increase freedom of movement and performance. But these advanced prostheses are extremely expensive (Currie et al., 2017). In recent years, the developments in 3D printing and easy prototyping techniques have provided cheap alternatives, enabling the production of 3D printed transradial prostheses with low costs. Prostheses give amputated individuals a chance to live their daily lives without needing any help by restoring the activities of daily living.

In daily life, people use different hand movements and an accurate prediction of the movement that a person wants to do is essential for the initiation of the correct movement. Since limb movements are caused by muscle contractions, EMG has emerged as a viable option for classification (Meier, 2004). EMG is a measurement method for a response or electrical activity of muscles in response to an action potential from nerves. The use of EMG signals for actuation of prosthetics is started in 1948. Different approaches such as on/off, proportional, direct, finite state, pattern recognition-based myoelectric control schemes are used in the use of EMG signals in prosthetic actuation (Geethanjali, 2016).

In a pattern recognition-based approach, it is important that EMG signals are successfully processed and classified for the prosthesis to perform the correct movement. An accurate classification requires signal acquisition, filtering, pre-processing, feature extraction and classification as shown in Figure 1.1.

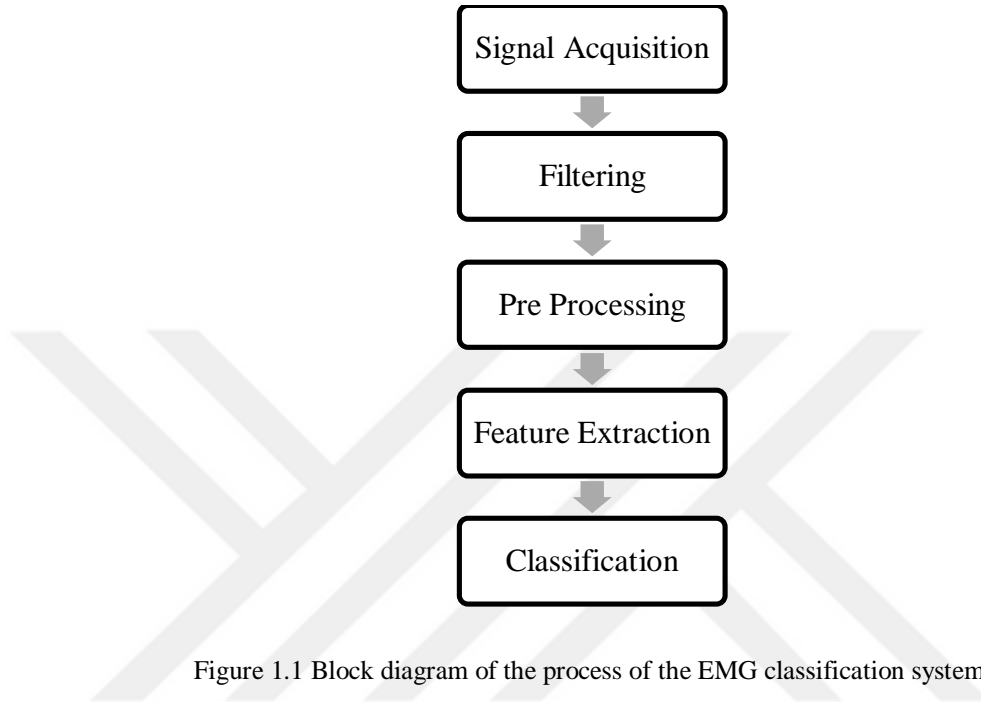


Figure 1.1 Block diagram of the process of the EMG classification system

When a small number of signal acquisition points are set, pattern recognition algorithms are beneficial for classifying a person's intention to actuate prosthetic, as they extract a set of characteristic features from the EMG signals. Studies in the 1990s have demonstrated over 90 % classification accuracy with various EMG time-domain features and classifiers (Englehart, Hudgins, Parker, & Stevenson, 1999; Zardoshti-Kermani, Wheeler, Badie, & Hashemi, 1995).

Studies also demonstrated that the utilization of different classifier types does not have a significant effect on classification by means of accuracy yet feature selection affects the accuracy rates significantly (Hargrove, Englehart, & Hudgins, 2007).

In this study, it is aimed to perform classification with high accuracy by examining the effect of hidden layer node number and different time-domain features of 2 channel EMG signals on the accuracy of classification via an artificial neural network (ANN).

In this context, individual accuracy rates of different time-domain properties were found. Based on individual accuracy rates, 2 feature sets were created. The feature sets, hidden layer node counts and classification algorithms were tested individually.

The structure of the thesis is described as follows In Chapter 2, the human anatomy is shortly explained with a thorough review of the anatomical plane descriptions, muscle physiology, skeletal muscle structure, and transradial amputation procedure. The design of this study is explained in detail in Chapter 3. The results of this study are given in Chapter 3.5 .



CHAPTER TWO

HUMAN ANATOMY

Anatomical planes, fundamental information about muscle physiology and skeletal muscle structure are given in this chapter. Finally, the appropriate surgical procedure for transradial amputation is explained.

2.1 Anatomical Planes

It is assumed that the body is divided into real and hypothetical slices called sections or planes (Figure 2.1). The term "section" refers to an actual cut or slice defined for studying the internal anatomy (Moore, Dalley, & Agur, 2013). On the other hand, the term "plane" refers to a flat surface that passes through the body which divides the body into two parts. There are three major anatomical planes as sagittal, frontal, and transverse (Dopico, 2016).

A sagittal plane divides the body and organs into two portions as right and left bypassing them vertically. If a sagittal plane divides the body or organs into equal portions, this plane is also called a median (midsagittal) plane (Currie et al., 2017). The most common use of this anatomical plane is studying portions of the head and pelvic organs (Saladin, 2010).

Another vertically extended plane is called the frontal (coronal) plane. However, this plane described as perpendicular to the sagittal planes thus it divides the body or organs into the front (anterior) and back (posterior) portions (Jenkins, 2009). The thoracic and abdominal cavities are most commonly illustrated in the frontal plane (Saladin, 2010).

For the purpose of examining the upper (superior) and lower (inferior) portions of the body or an organ, the transverse (horizontal) plane is preferred. This plane divides the body or an organ into two portions by passing by perpendicular to its long axis (Moore et al., 2013; Saladin, 2010).

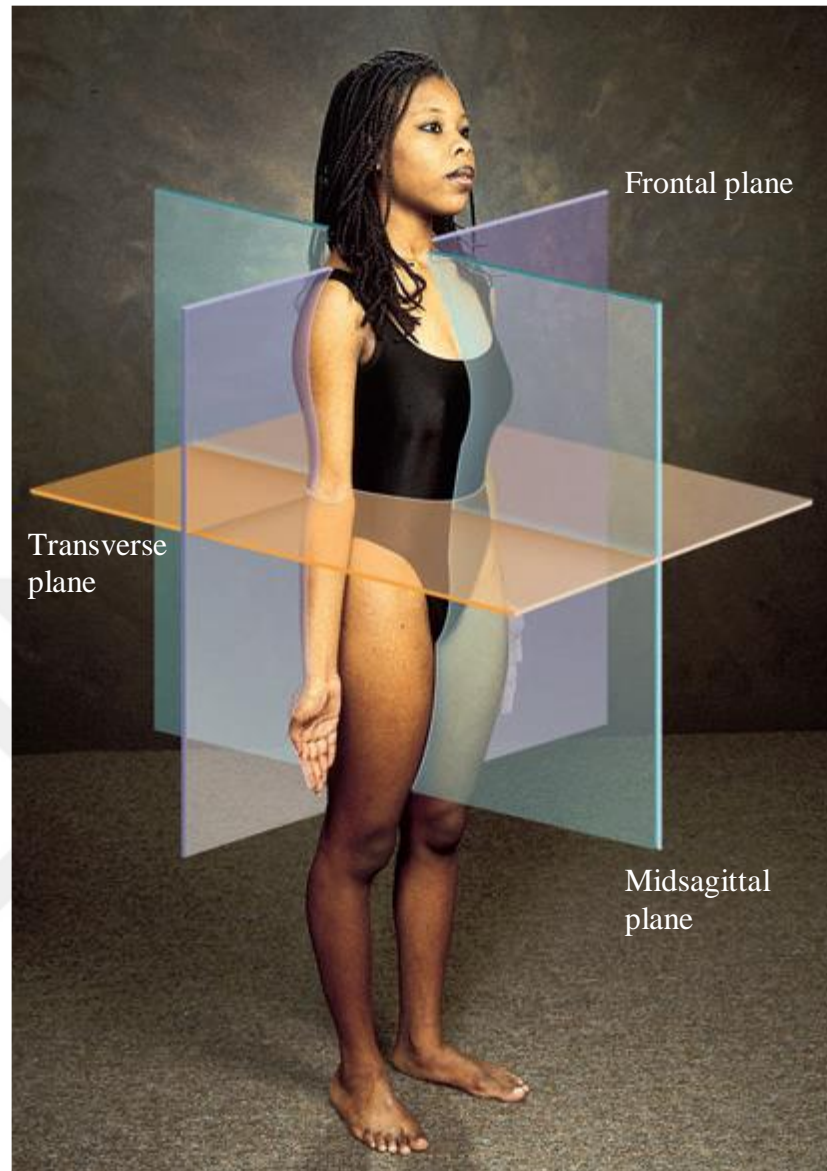


Figure 2.1 Anatomical planes (Saladin, 2010)

When the motions are examined in anatomy, planar terms are used (Figure 2.2). Table 2.1 shows directional terms. When talking about the movement direction of the limbs in the body, the terms in this table are used.

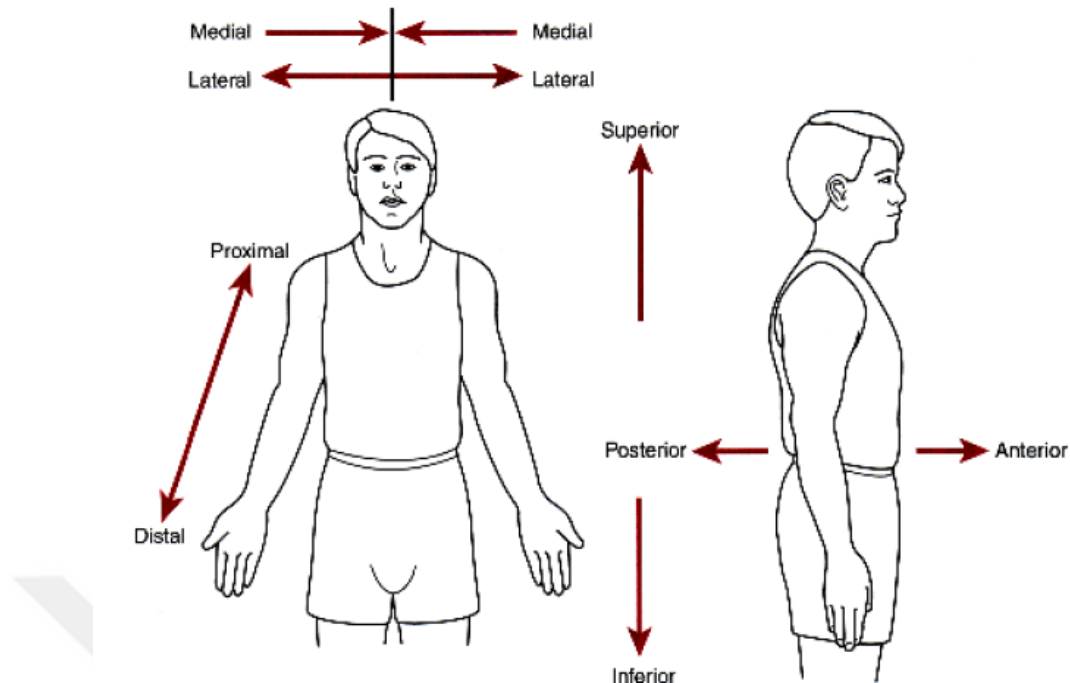


Figure 2.2 Illustration of directional terms in human anatomy (Luksch, 2010)

Table 2.1 Directional terms in human anatomy (Saladin, 2010)

Term	Meaning
Ventral	Toward the front* or belly
Dorsal	Toward the back or spine
Anterior	Toward the ventral side*
Posterior	Toward the dorsal side*
Superior	Above
Inferior	Below
Medial	Toward the median plane
Lateral	Away from the median plane
Proximal	Closer to the point of attachment or origin
Distal	Farther from the point of attachment or origin
Superficial	Closer to body surface
Deep	Farther from the body surface

*Definitions given for human it may differentiate for other animals

2.2 Muscle Physiology

Muscle cells consist of protein filaments called actin and myosin. Muscle contraction is produced by sliding past of these two filaments each one other. These contractions change the length and shape of the cell. Muscles produce force and motion as the main function of these contractions. Muscles have a wide variety of functions such as posture stability, changing of posture, locomotion, as well as movements of internal organs, such as the peristaltic movement of intestines in the digestive system, or contraction of the heart muscles in the circulatory system for pumping blood from the heart to the whole body.

2.2.1 Muscle Types

The human body consists of three different muscle types as skeletal (voluntary), cardiac (myocardium) and smooth (involuntary) which differ in their forms and functions.

The skeletal muscle is affixed to the bone via tendons and mainly functions for locomotion and posture conservation. Although control of posture conserved as an automatic reflex, the skeletal muscle functions for conscious movements like non-postural muscles

The smooth muscle is responsible for the unconscious and automatic reflexive movements of organs such as the bladder, stomach, intestines, and blood vessels. The smooth muscles do not have a conscious control mechanism.

The cardiac muscle can be seen only in the heart. The cardiac muscle has a similar structure with skeletal muscle, yet it from skeletal muscles differs by its uncontrollable unconscious contractions.

2.3 Skeletal Muscle Structure

Epimysium and perimysium are connective tissues that surround the skeletal muscles (Figure 2.3). The epimysium surrounds the skeletal muscle from the outside and the perimysium encapsulates the fiber bundles (Frontera & Ochala, 2015). Each muscle fiber has a diameter of approximately 100 μm and a length of 1 cm. Cell

membrane or myolemma surrounds these fibers (Frontera & Ochala, 2015). There are several protein complexes physically attached to the internal myofilament structure in relation to the sarcolemma; particularly in the thin filament for the actin protein. (Frontera & Ochala, 2015).

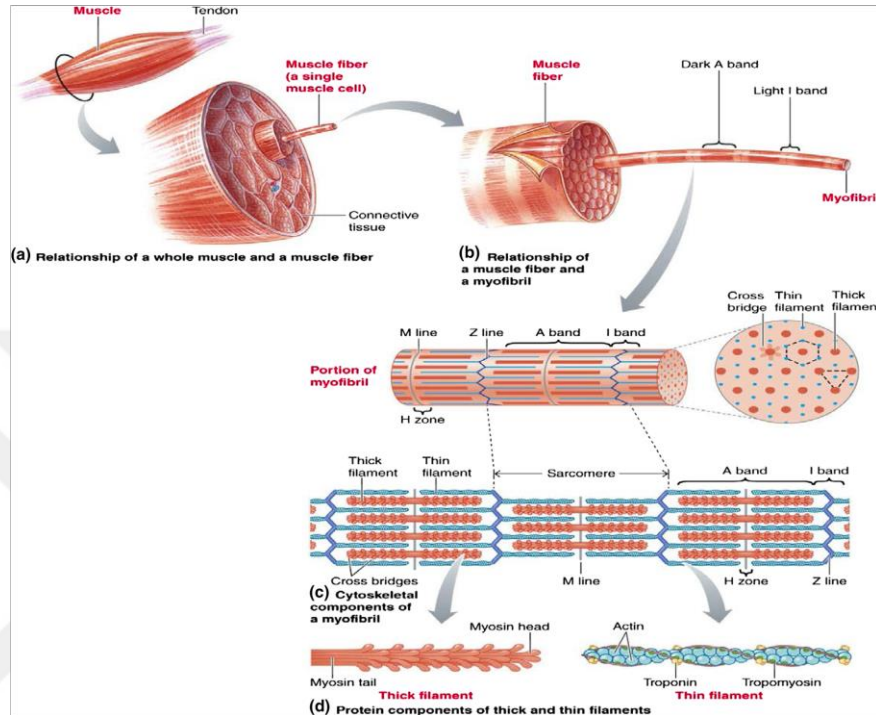


Figure 2.3 Structure of skeletal muscle (Frontera & Ochala, 2015)

2.3.1 Forearm Muscles

Tendons in the forearm are connected to the wrist, hand, and fingers. The tendons extend across the arm from the distal part of the forearm to the wrist, hand, and fingers (Moore et al., 2013). The forearm flexors and pronators are located in the anterior part and are mainly stimulated by the median nerve (Moore et al., 2013). On the other hand, radial nerve stimulates the extensors and supinators of the forearm (Hadley, 2007).

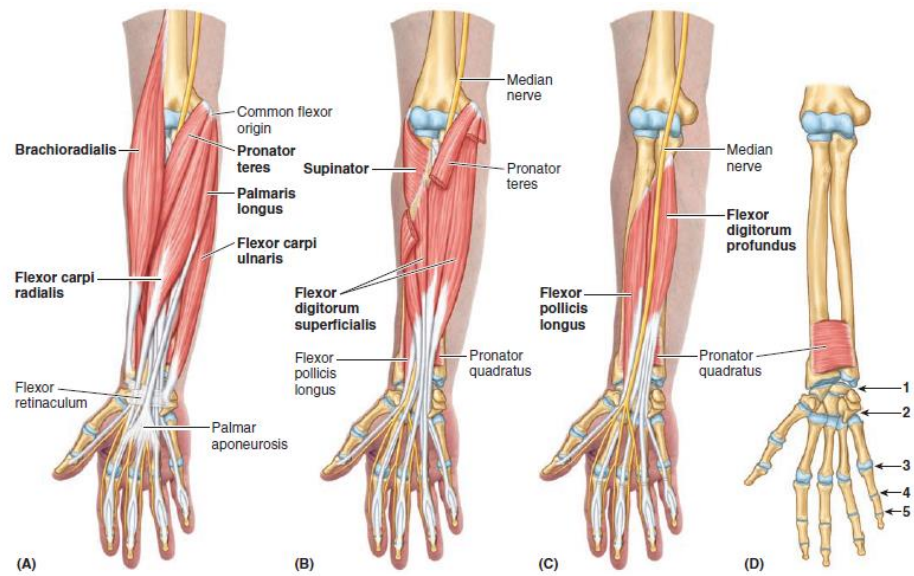


Figure 2.4 Muscles of the anterior portion of the forearm. A) First layer B) Second layer C) Third layer D) The fourth layer (Hadley, 2007)

The muscular system consists of several layers. Each layer has different muscle groups with different functions (Figure 2.4). The origin, insertions, the nerves to which they are triggered by and the functions of the muscles in the lower arm vary (Table 2.2).

Table 2.2 Transradial arm muscles and their properties (K. Chung & H. Chung, 2008)

Muscle	Origin	Insertion	Nerve	Action
Pronator Teres	Medial epicondyle and coronoid process of ulna	Middle of the lateral side of the radius	Median	Pronates and flexes the forearm
Flexor Carpi Radialis	Medial epicondyle of humerus	Bases of second and third metacarpals Flexor	Median	Flexes forearm, flexes and abducts hand
Palmaris Longus	Medial epicondyle of the humerus	retinaculum, palmar aponeuroses	Median	Flexes forearm and hand
Flexor Carpi Ulnaris	Medial epicondyle (humeral head); medial olecranon, and posterior border of ulna (ulnar head)	Pisiform, the hook of hamate, and base of the fifth metacarpal	Ulnar	Flexes forearm; flexes and adducts hand
Flexor Digitorum Superficialis	Medial epicondyle, coronoid process, oblique line of radius	Middle phalanges of the finger	Median	Flexes proximal interphalangeal joints, flexes hand and forearm
Flexor Digitorum Profundus	Anteromedial surface of ulna, interosseous membrane	Bases of distal phalanges of fingers	Ulnar and median	Flexes distal interphalangeal joints and hand
Flexor Pollicis Longus	The anterior surface of the radius, interosseous membrane, and coronoid process	The base of distal phalanx of thumb	Median	Flexes thumb
Pronator Quadratus	Anterior surface of distal ulna	Anterior surface of distal radius	Median	Pronates forearm

2.4 Transradial Amputation

Transradial forearm amputation is a very common upper limb amputation (Smith, Kuiken, & Hargrove, 2015). The remaining soft tissue and muscle tissue should provide sufficient tissue coverage for the radius and ulna.

Figure 2.5 shows photographs of the operation site of the healed patient after successful transradial amputation.



Figure 2.5 A healed post transradial amputation patient (Marchessault, McKay, & Hammert, 2011)

Myodesis and myoplasty techniques are widely used in procedures in amputation surgeries. Myodesis and myoplasty techniques simply distinct by the suture anchor of the muscle. In myodesis technique, muscle or tendon needs to be sutured to the bone for stabilization yet in myoplasty technique; the muscle needs to be sutured to another muscle. During an amputation, bone-on-muscle movement avoidance and steady bone coverage are essential to reduce bursitis risk and these are secured by the application of myodesis technique for the transradial arm muscles to the radius and ulna bones (Marchessault et al., 2011; Stanos & Rivers, 2014). On the other hand, application myoplasty technique between the superficial flexor muscles and extensor muscles may be preferred, if the patient has poor vascular health (Marchessault et al., 2011; Stanos & Rivers, 2014). Myoplasty technique provides sufficient tension to allow the contraction of the muscles after closure (Currie et al., 2017; Marchessault et al., 2011). However, for transradial amputation, both myodesis and myoplasty techniques are combined for the accomplishment of soft tissue coverage.

Transradial amputation consists of five main steps (Figure 2.6). In the first step of the operation, a fishmouth incision is applied to the forearm (A). Deep and superficial flexor muscles are separated as well as extensor muscles (B) (Marchessault et al., 2011). Muscle stabilization to bone by suture according to

myodesis technique (C). Muscle stabilization of superficial flexors and extensors to each other by suture according to myoplasty technique (D) (Marchessault et al., 2011). Muscles contoured with myofascial sutures to secure closure without excessive tension (E) (Currie et al., 2017; Marchessault et al., 2011).

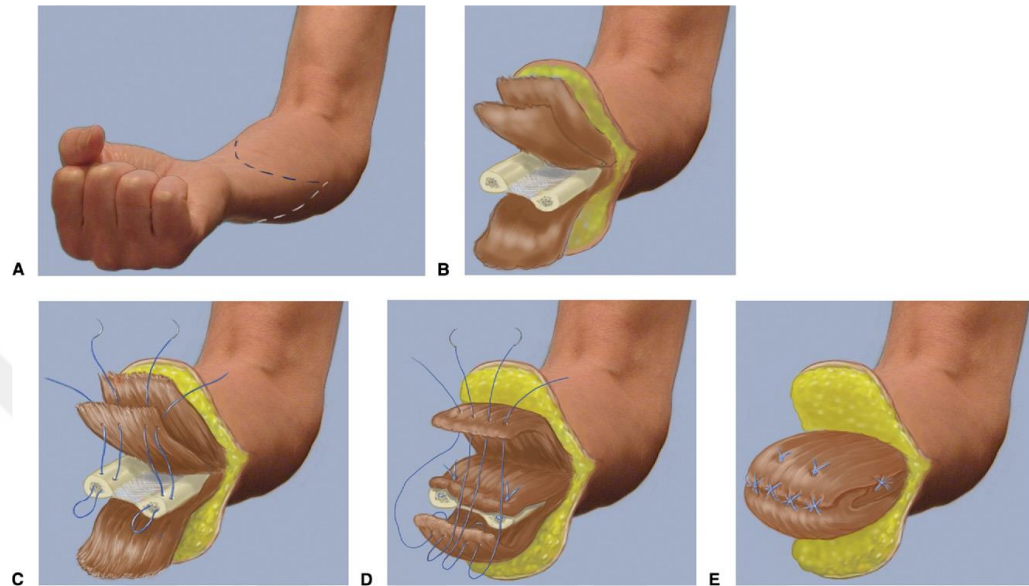


Figure 2.6 Illustration of transradial amputation. A: Fishmouth incision B: Muscle separation C: Myodesis technique D: Myoplasty technique E: Myofascial closing (Marchessault et al., 2011)

CHAPTER THREE

DESIGN OF STUDY

This chapter includes the equipment used for signal acquisition, electrode placement, signal acquisition, signal processing, feature extraction, and feature selection (Figure 3.1).

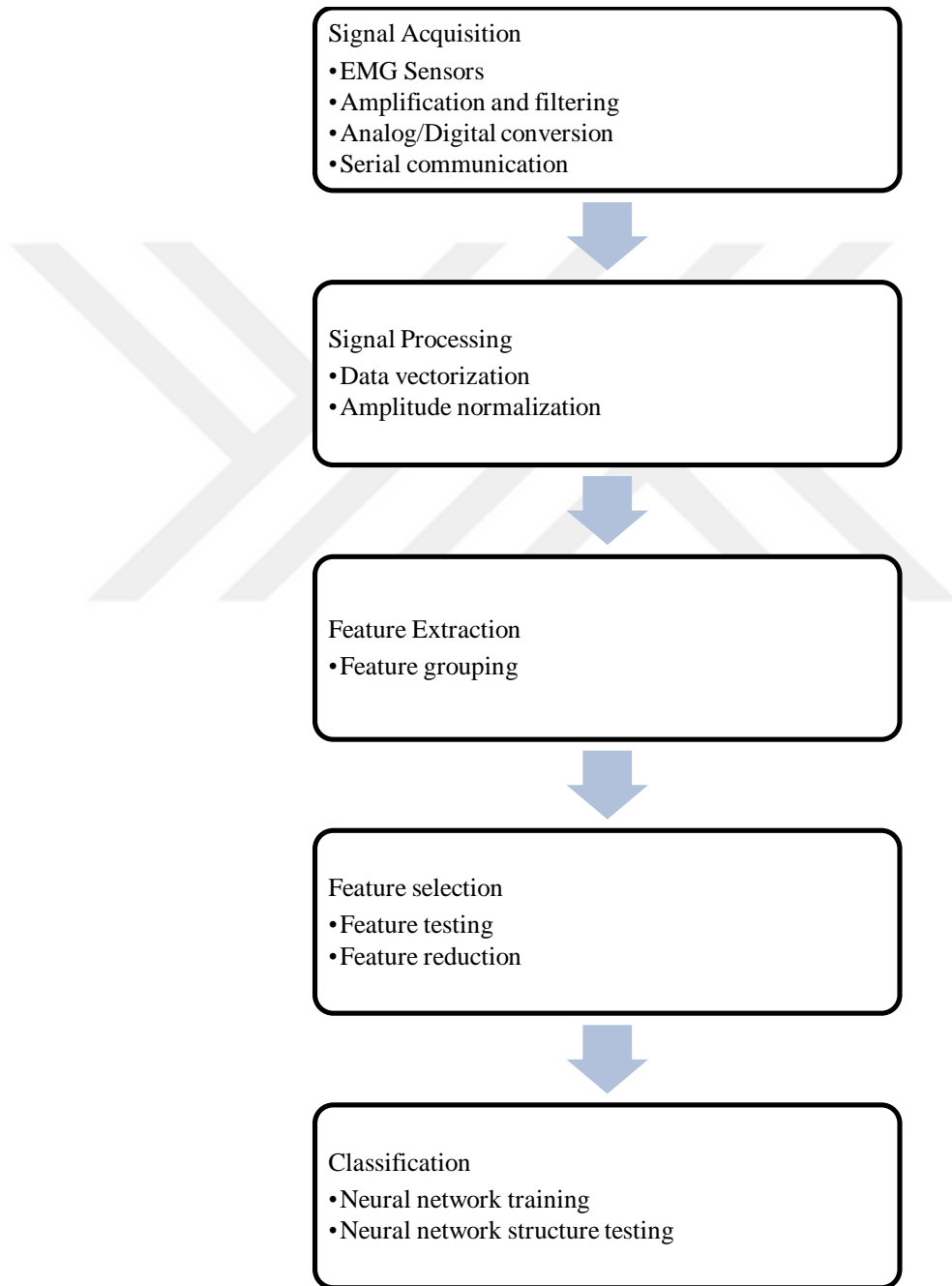


Figure 3.1 Block diagram of study

3.1 EMG Sampling Equipment

The Myoware Muscle Sensor (AT-04-001), HC-06 Bluetooth Communication Module and Arduino Mini Pro Leonardo microcontroller were used as hardware to obtain EMG signals and transfer them to a computer.

Arduino is a physical programming platform consisting of an input/output board and a development environment that includes an implementation of the processing/wiring language (Arduino, n.d.).

The difference of Arduino Leonardo from other cards is built-in communication capability with a universal serial bus (USB) of the ATmega32u4 microcontroller (Arduino, 2018). Therefore, it does not require a second processor.

Arduino Leonardo has 20 digital input/output pins. 7 of them can be used as pulse width modulation (PWM) outputs and 12 of them can be used as analog inputs (Arduino, 2018). There is also a 16 MHz crystal oscillator, USB connection, power jack (2.1mm), in-circuit serial programming (ICSP) header and reset button (Arduino, 2018). Arduino Leonardo contains all of the components necessary to support a microcontroller (Arduino, 2018).

EMG has conventionally been used for diagnosis and medical research by the measurement of muscle activation by electrical potential (Sparkfun, 2019). The rapid development of technology has made microcontrollers more powerful and the capacity of integrated circuits greater. Due to development in this field, the use of EMG circuits and sensors in prosthetic and robotic control systems has started to become widespread.

In this study, Advancer Technologies' Myoware™ Muscle Sensor (AT-04-001) (Figure 3.2) is used as an EMG sensor for EMG signal acquisition.



Figure 3.2 Myoware EMG Sensor (Sparkfun, 2015)

The MyoWare Muscle Sensor has a wearable design that allows the user to attach biomedical sensor pads directly to the board itself. This board also includes features including, a single-supply voltage of +3.1V to +5V, raw EMG output, polarity protected power pins, indicator LEDs, and an on/off switch. Figure 3.3 shows the sensor layout of the EMG sensor (Sparkfun, 2019).

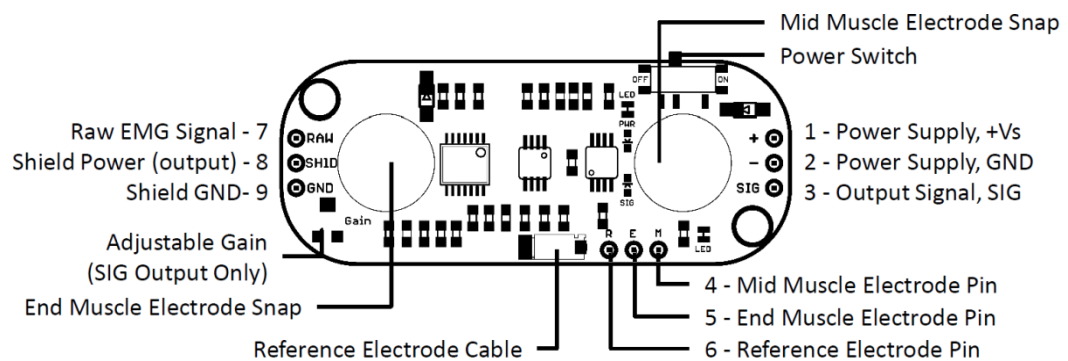


Figure 3.3 Sensor layout (Sparkfun, 2015)

The correct placement of the EMG electrodes is essential for acquiring sufficient and relatively clean signals. When the electrodes are placed in the direction of the

muscle fibers and in the middle of the muscle body, they give the most accurate results. Misplacement of the sensor reduces the strength and quality of the signal obtained due to reduced measured values and increased interference due to cross-interference. The correct sensor placement is shown in Figure 3.4.

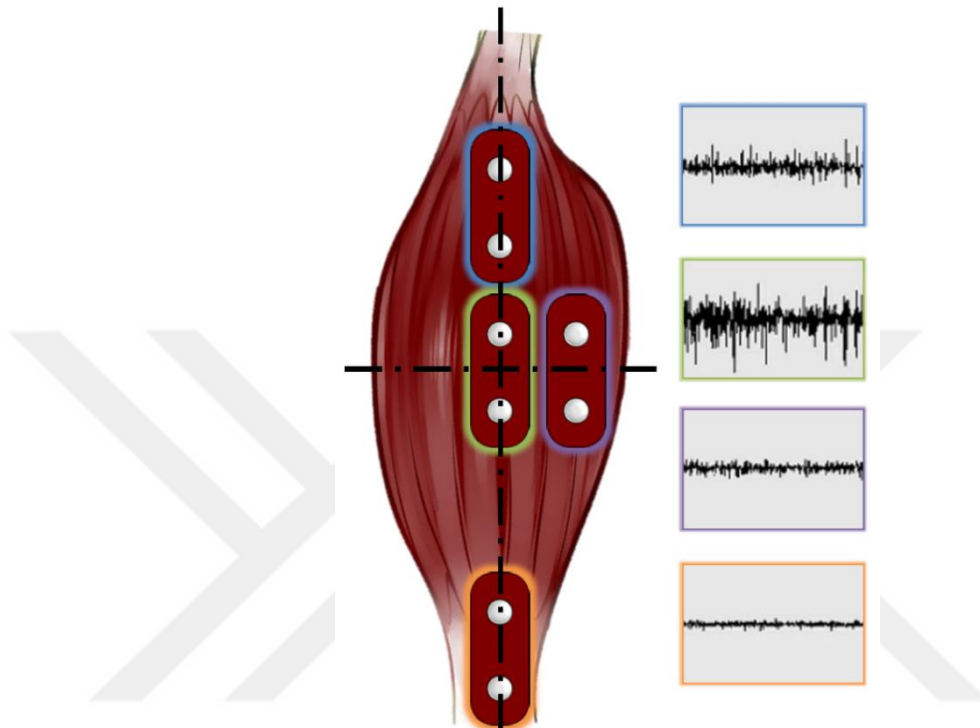


Figure 3.4 Sensor placement blue - innervation zone, green – correct placement, purple – midline offset, orange – myotendon junction (Sparkfun, 2015)

Arduino software was used to transfer the data received from the EMG sensor to the computer via Bluetooth. The serial communication method was preferred for receiving the values from the EMG sensor. The HC-06 Bluetooth module was used to communicate between the Arduino and the computer.

3.2 Signal Acquisition

Brain tissue and muscle tissue might be called sensitive tissues. In response to proper stimuli, both tissues may generate electrical signals or may transmit signals (Joochim & Siriwatcharakul, 2019). Monitoring and recording of the signals produced by these tissues are of great importance both for clinical and engineering purposes. EMG has a broad application such as diagnosis of health issues,

developing brain-computer interfaces, rehabilitation, and control of prosthetics (Al-Ani, Koprinska, Naik, & Khushaba, 2016).

EMG is a commonly used noninvasive method for monitoring and recording the electrical activity of the skeletal muscles (Al-Ani et al., 2016). EMG signals may be acquired by non-invasive surface electrodes or invasive intramuscular fine wire (Chowdhury et al., 2013). Placing a thin wire into the muscle allows the recording of the EMG signal from the deeper parts of the muscle. However, inserting the needle into the casing is a painful operation for the person and requires a clinical assistant (Tengku Zawawi et al., 2018). Since noninvasive methods provide signal acquisition without causing any pain or harm to the person due to clinical operation, it is preferably used to control powered prosthetics (Al-Ani et al., 2016). This control method of prosthetics defined as myoelectric control (Jiang, Vest-Nielsen, Muceli, & Farina, 2012). The EMG is based on the principle of the measurement of the electrical potential between the two ends of the muscle during the contraction of muscles (Reaz, Hussain, & Mohd-Yasin, 2006).

In order to record EMG signals of related movements, the first EMG sensor was placed on flexor carpi ulnaris and the second one was placed on extensor carpi radialis longus muscles (Khushaba, Al-Timemy, Al-Ani, & Al-Jumaily, 2017). Sensors were located as shown in Figure 3.5. Data received with the Myoware EMG sensor was recorded by Arduino and then transferred MATLAB via Bluetooth. The study was conducted with the participation of 10 subjects. The same movement was repeated 50 times in each recording session. At the end of the recording session, a 50x100 data matrix with 50 repetitions of the same motion was recorded. During recording sessions, the user is alerted by a beep sound and then makes his/her hand relax after performing the movement and repeats the movement when he/she hears the sound again.

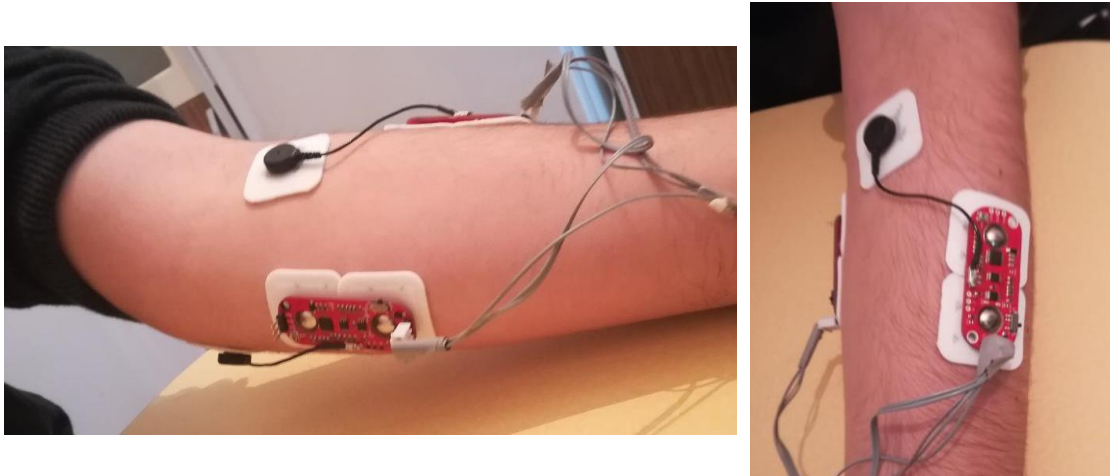


Figure 3.5 Positioning of EMG electrodes (Personal archive, 2019)

3.3 Signal Processing

Minimum – maximum normalization is applied to EMG signals (Figure 3.6).

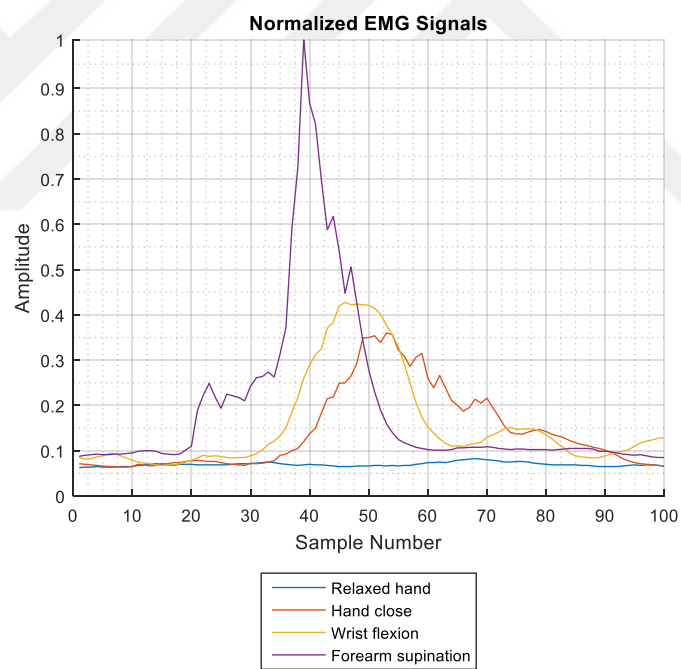


Figure 3.6 EMG signals with minimum-maximum normalization

3.4 Feature Extraction

In order to achieve high classification accuracy, features must be extracted from the data. MAV, RMS, LOG, SSI, VAR, MFL, WL, AAC, DASDV, WAMP and SSC features are used for this study.

Time-domain features provide different information such as energy information, complexity information and frequency information (Phinyomark, Phukpattaranont, & Limsakul, 2012). In this thesis, features are investigated in these three groups. Group 1, energy information, consists of MAV, RMS, LOG, SSI, VAR, and MFL features. Group 2, complexity information, consists of WL, AAC and DASDV features. Group 3, frequency information, consists of WAMP and SSC features. Estimation of the feature value of the signal, x_i , in segment i which is N discrete samples in length is expressed as in Table 3.1.

The raw EMG amplitude of the different movements and the Feature amplitudes corresponding to these movements are given in Figure 3.7 and Figure 3.8. Sample numbers between 0-100, 200-300, 400-500 and 600-700 represent a relaxed hand. The hand closing movement is represented between sample numbers between 100 and 200. In the same manner, the wrist flexion movement is represented with sample numbers between 300 and 400. Finally, forearm supination movement is represented 500-600 sample number interval

Table 3.1 Feature groups and mathematical representations

Feature Group	Feature	Equation
Energy Information (EI)	MAV	$\text{MAV} = \frac{1}{N} \sum_{i=1}^N x_i $
	RMS	$\text{RMS} = \sqrt{\frac{1}{N} \sum_{i=1}^N x_i^2}$
	LOG	$\text{LOG} = e^{\frac{1}{N} \sum_{i=1}^N \log(x_i)}$
	SSI	$\text{SSI} = \sum_{i=1}^N x_i^2$
	VAR	$\text{VAR} = \frac{1}{N-1} \sum_{i=1}^N x_i^2 $
Complexity Information (CI)	MFL	$\text{MFL} = \sum_{i=1}^{N-1} (x_{i+1} - x_i)^2$
	WL	$\text{WL} = \sum_{i=1}^{N-1} x_{i+1} - x_i $
	AAC	$\text{AAC} = \frac{1}{N} \sum_{i=1}^{N-1} x_{i+1} - x_i $
	DASDV	$\text{DASDV} = \sqrt{\frac{1}{N-1} \sum_{i=1}^{N-1} (x_{i+1} - x_i)^2}$
Frequency Information (FI)	WAMP	$\text{WAMP} = \sum_{i=1}^{N-1} [f(x_i - x_{i+1})]$ $f(x) = \begin{cases} 1, & \text{if } x \geq \text{threshold} \\ 0, & \text{otherwise} \end{cases}$
	SSC	$\text{SSC} = \sum_{i=2}^{N-1} [f(x_i - x_{i-1}) \times f(x_i - x_{i+1})]$ $f(x) = \begin{cases} 1, & \text{if } x \geq \text{threshold} \\ 0, & \text{otherwise} \end{cases}$

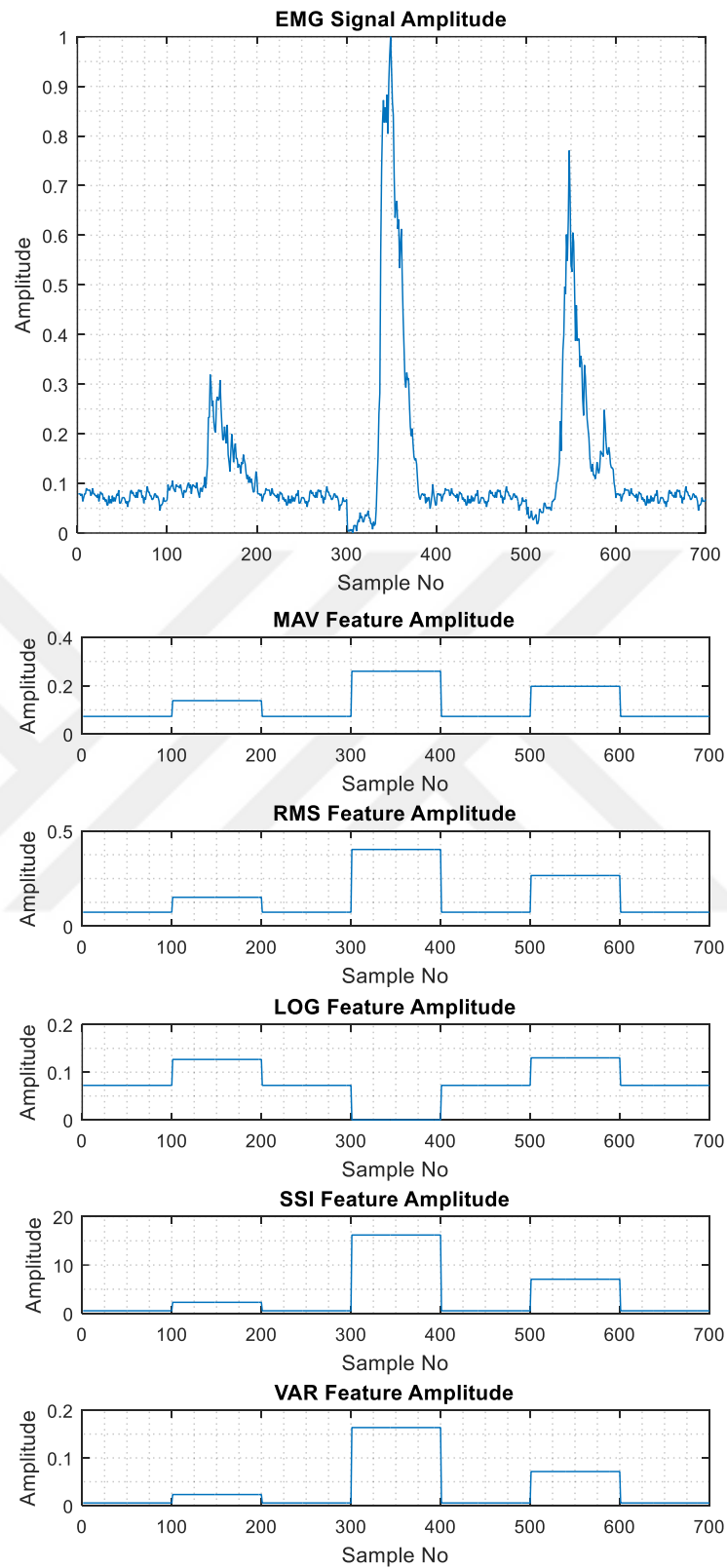


Figure 3.7 Amplitudes of raw EMG signal and energy information features for different movements

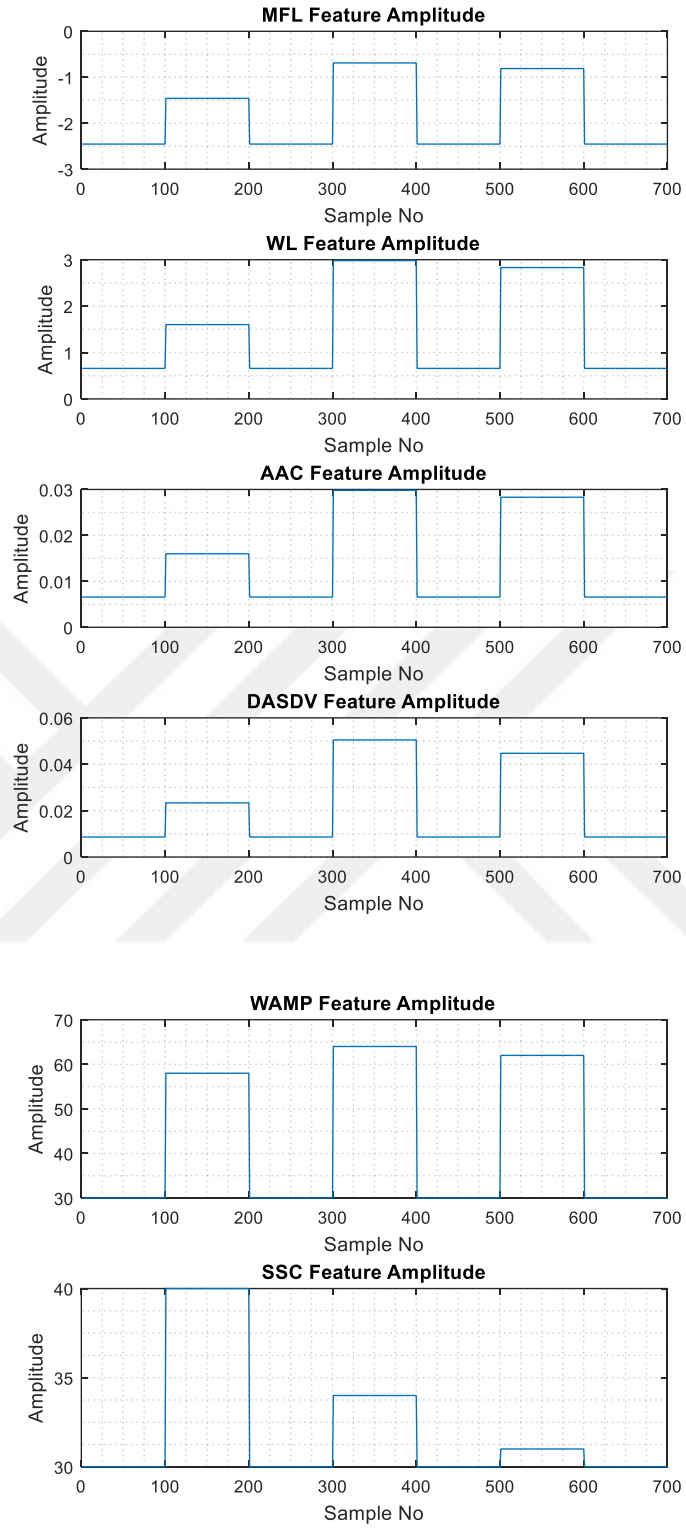


Figure 3.8 Amplitudes of complexity and frequency information features for different movements

3.4.1 Energy Information

3.4.1.1 Mean Absolute Value (MAV)

MAV is one of the simplest features that can be used for data. It is defined as the sum of each instance in the data set divided by the number of instances (Phinyomark et al., 2012).

3.4.1.2 Root Mean Square (RMS)

The RMS feature is another feature that provides energy information of the signal. It is modeled as a Gaussian random process modulated in amplitude, which relates to constant force and non-fatiguing contraction (Caesarendra, 2018).

3.4.1.3 Log Detector (LOG)

The LOG feature gives an estimate of muscle contraction force using the logarithm and log detector (Tkach, Huang, & Kuiken, 2010).

3.4.1.4 Simple Square Integral (SSI)

The SSI represents the energy of the signal. It is the summation of the squared values of EMG signal amplitude (Phukan, Kakoty, Shivam, & Gan, 2019).

3.4.1.5 Variance of EMG (VAR)

The VAR feature is another energy index. Generally, the variance is defined as an average of square values of the deviation of that variable (Phinyomark, Hirunviriyaya, Limsakul, & Phukpattaranont, 2010).

3.4.2 Complexity Information

3.4.2.1 Maximum Fractal Length (MFL)

The MFL feature is defined as a measure of the strength of muscle contraction in a logarithmic scale (Arjunan & Kumar, 2010).

3.4.2.2 Waveform Length (WL)

The WL feature provides information about the complexity of the EMG signal. This feature is described as the total length of the waveform over a time period (Phinyomark et al., 2010).

3.4.2.3 Average Amplitude Change (AAC)

The AAC feature is another method that provides information about the complexity of the EMG signal and almost identical to the WL, except that wavelength is averaged (Phinyomark et al., 2012).

3.4.2.4 Difference Absolute Standard Deviation Value (DASDV)

The DASDV is similar to the RMS feature (Yu, Jeong, Hong, & Lee, 2012). However, DASDV is defined as the standard deviation value of wavelength (Phinyomark et al., 2012; Yu et al., 2012).

3.4.3 Frequency Information

3.4.3.1 Willison Amplitude (WAMP)

The WAMP feature is related to muscle contraction as the LOG feature. However, it is described as a number of times resulting from the difference between the signal amplitude among a pair of adjacent segments that exceed a defined threshold. A threshold value of 75 mV has been chosen (Zardoshti-Kermani et al., 1995).

3.4.3.2 Slope Sign Change (SSC)

The SSC feature is another method that provides information about the frequency of the EMG signal. It is defined as a number of times that the slope of the EMG signal changes sign (Hudgins, Parker, & Scott, 1993). A threshold value of 15 mV has been chosen (Hudgins et al., 1993).

3.4.4 MATLAB Functions

MATLAB was used to process and classify the data recorded on the computer via Bluetooth. The codes for feature extraction are given in Table 3.2.

Table 3.2 MATLAB codes for feature extraction

Feature	MATLAB Code
MAV	MAV=mean(abs(A));
RMS	MS=sqrt(mean(A.^2));
LOG	N=length(A); B=0; for k=1:N B=B+log(abs(A(k))); end LOG=exp(B/N);
SSI	SSI=sum(A.^2);
VAR	N=length(A); VAR=(1/(N-1))*sum(A.^2);
MFL	N=length(A); B=0; for n=1:N-1 B=B+(A(n+1)-A(n))^2; end MFL=log(sqrt(B));
WL	N=length(A); WL=0; for i=2:N WL=WL+abs(A(i)-A(i-1)); end
AAC	N=length(A); B=0; for i=1:N-1 B=B+abs(A(i+1)-A(i)); end AAC=B/N;
DASDV	N=length(A); B=0; for i=1:N-1 B=B+(A(i+1)-A(i))^2; end DASDV=sqrt(B/(N-1));
WAMP	N=length(A); WA=0; for k=1:N-1 if abs(A(k)-A(k+1)) >= thres WA=WA+1; end end
SSC	N=length(A); SSC=0; for i=2:N-1 if ((A(i) > A(i-1) && A(i) > A(i+1)) (A(i) < A(i-1) && A(i) < A(i+1))) ... && ((abs(A(i)-A(i+1)) >= thres) (abs(A(i)-A(i-1)) >= thres)) SSC=SSC+1; end end

3.5 Feature Selection

Extracted features were used as input vector in ANN training separately to determine the individual accuracies of these features. In these trials, a different number of hidden layer neurons were tested. In the process of feature selection,

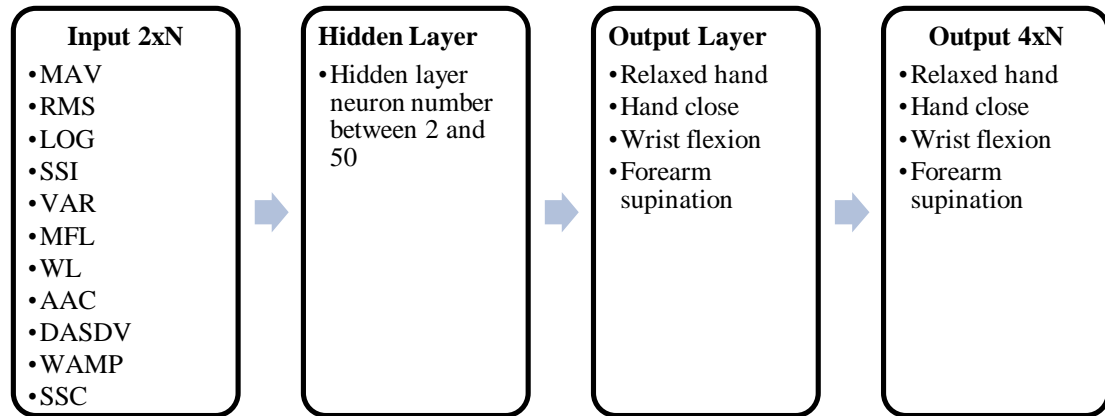
accuracy is used as a performance metric. However, accuracy, sensitivity, specificity, and precision performance metrics are used for the performance evaluation of feature sets (Table 3.3).

Table 3.3 Performance metrics

Accuracy % = $\frac{\text{True Positive} + \text{True Negative}}{\text{Sample Size}} \times 100$
Sensitivity = $\frac{\text{True Positive}}{\text{True Positive} + \text{False Negative}}$
Specificity = $\frac{\text{True Negative}}{\text{True Negative} + \text{False Positive}}$
Precision = $\frac{\text{True Positive}}{\text{True Positive} + \text{False Positive}}$

The first trial was conducted with Scaled Conjugate Gradient (SCG) as a training function and cross-entropy as a performance function. All features were tested with even numbers of hidden layer neurons between 2 and 50 (Figure 3.9). MAV feature from group 1 has given the best accuracy rate and followed by the RMS feature. MFL feature from group 2 has given the best accuracy rate and followed by the DASDV feature. SSC feature from group 3 has given the best accuracy (Table 3.4 & Table 3.5 & Figure 3.13).

The effect of the hidden layer neuron number on accuracy was investigated separately for 3 feature groups. For EI group features, after the number of hidden layer neurons (HLN) exceeded 40, no significant increase in accuracy was observed (Figure 3.10). Compared to the EI group, the increase in the number of hidden layer neurons had less effect on the CI group. After the number of neurons exceeded 10, there was no significant increase in accuracy (Figure 3.11). When the FI group was considered, an accuracy graph is obtained which is almost independent of the number of hidden layers (Figure 3.12).



Training Function: Scaled Conjugate Gradient

Input: 1 feature x 2 channel

Figure 3.9 Structure of ANN training with SCG function

Table 3.4 Mean accuracy of 10 SCG train trials for EI Group

HLN	Accuracy \pm Std % - EI Group				
	MAV	RMS	LOG	SSI	VAR
2	37.4 \pm 2.3	38.7 \pm 1.1	36.1 \pm 1.3	37.8 \pm 1.4	37.4 \pm 1.8
4	42.2 \pm 2.5	41.9 \pm 1.9	43 \pm 3.7	42.2 \pm 3.1	37.8 \pm 3.9
6	45.8 \pm 3.7	45.6 \pm 3.2	47.5 \pm 0.9	41.7 \pm 3.4	39.1 \pm 3.3
8	50 \pm 1.7	46.9 \pm 2.7	48.2 \pm 3.6	46.6 \pm 1.2	43.1 \pm 1.9
10	48.3 \pm 1.7	45.8 \pm 4.4	49 \pm 1.8	42.3 \pm 4.6	43.6 \pm 3.3
12	49.1 \pm 1.7	52.2 \pm 2	50.8 \pm 2.6	44.7 \pm 2.4	45.8 \pm 0.9
14	49.5 \pm 2.5	48.3 \pm 2.5	51.9 \pm 1.5	45.7 \pm 1.1	43.9 \pm 2.2
16	53.4 \pm 4.4	51.8 \pm 4.1	55.1 \pm 1.3	42.5 \pm 2.9	45 \pm 1.3
18	53.4 \pm 2.5	54.7 \pm 2.1	54.6 \pm 2.7	44 \pm 6.4	45.8 \pm 0.6
20	53.1 \pm 2.5	56.1 \pm 3.6	56 \pm 2.9	43.3 \pm 4.4	45.3 \pm 0.8
22	51.4 \pm 4.5	53.6 \pm 6.8	56.3 \pm 2.8	46.2 \pm 1.8	45.1 \pm 1.6
24	58.2 \pm 2.2	56.4 \pm 4.7	54.8 \pm 3.3	44.1 \pm 2.8	44.8 \pm 0.8
26	55.4 \pm 3.4	56.1 \pm 3.4	54.6 \pm 4.1	45 \pm 0.7	45.9 \pm 0.8
28	56.4 \pm 3.7	57.4 \pm 5.4	58.3 \pm 2.5	46.6 \pm 1.7	45.5 \pm 0.8
30	56.9 \pm 2.3	59.2 \pm 3.3	58.3 \pm 0.8	45.9 \pm 1.1	46.2 \pm 1
32	57.5 \pm 5.2	55.3 \pm 3.9	57.2 \pm 2.6	45.7 \pm 1.6	45.2 \pm 1.7
34	55.7 \pm 5.1	58.9 \pm 2.4	59.1 \pm 0.6	45.8 \pm 1.7	45.4 \pm 0.5
36	57.5 \pm 2.5	57.2 \pm 2.5	58.3 \pm 1	46.9 \pm 1.2	47.1 \pm 1.8
38	56.6 \pm 5.6	58.5 \pm 4	57.7 \pm 2	47.2 \pm 1.7	45.3 \pm 1.3
40	61.3 \pm 1.1	59 \pm 2.8	58.6 \pm 0.8	46.6 \pm 1.3	46.2 \pm 1.2
42	59.5 \pm 1.8	56.9 \pm 1.6	59 \pm 1.1	45.3 \pm 1.3	45.8 \pm 3.4
44	57.9 \pm 5.3	59 \pm 0.8	57.8 \pm 2.3	47 \pm 1.3	46 \pm 2
46	61.1 \pm 2.1	60.4 \pm 1.1	59.5 \pm 1.2	46.8 \pm 2	46.1 \pm 1.3
48	59.6 \pm 4	60.6 \pm 3.2	58.9 \pm 1	45.9 \pm 1.2	46.1 \pm 2.3
50	61.1 \pm 1.4	60.1 \pm 3.7	59.1 \pm 1.3	46.8 \pm 1	46.3 \pm 1.6

Table 3.5 Mean accuracy of 10 SCG train trials for the CI group and FI Group

HLN	Accuracy \pm Std % - CI Group				Accuracy \pm Std % - FI Group	
	MFL	WL	AAC	DASDV	WAMP	SSC
2	52.2 \pm 1.1	48.3 \pm 3.8	47.9 \pm 3	50.7 \pm 0.8	38.6 \pm 1.4	37.9 \pm 2.3
4	61.8 \pm 4.1	54.8 \pm 2.8	52.7 \pm 5.7	56.2 \pm 3.6	39.7 \pm 0.5	41.6 \pm 0.8
6	66.7 \pm 1.4	58.6 \pm 4	58 \pm 3.4	58.1 \pm 5.6	40.2 \pm 0.6	42 \pm 0.4
8	67.7 \pm 3.7	60.2 \pm 1.8	59 \pm 3.1	57.9 \pm 4.5	40.4 \pm 0.6	42.1 \pm 0.4
10	68.5 \pm 1.4	60.9 \pm 2.5	59.5 \pm 3.8	63.4 \pm 1.8	40.4 \pm 1.4	42.1 \pm 0.5
12	69.2 \pm 0.5	62.7 \pm 2.8	63.6 \pm 1.1	61.6 \pm 3.9	41.2 \pm 0.5	42.7 \pm 0.6
14	70.1 \pm 0.2	61.8 \pm 3.5	62.5 \pm 5.1	63.1 \pm 2.8	41.5 \pm 0.6	43.3 \pm 0.2
16	69.6 \pm 0.3	62.8 \pm 1.2	64.6 \pm 1.3	65.3 \pm 1.4	40.6 \pm 0.8	42.7 \pm 0.5
18	69.7 \pm 0.4	64.3 \pm 1.5	64 \pm 1	64.1 \pm 2.8	41.9 \pm 0.6	42.7 \pm 0.6
20	69.8 \pm 0.5	64.6 \pm 1.2	63.1 \pm 1.3	65.1 \pm 1.8	41.9 \pm 0.7	43.2 \pm 0.4
22	70.6 \pm 0.3	64.6 \pm 1.6	64.1 \pm 2.1	65.5 \pm 3.3	41.8 \pm 0.6	42.8 \pm 1.3
24	70.3 \pm 0.6	64.9 \pm 1.7	64.5 \pm 0.9	65.3 \pm 2.1	41.8 \pm 0.8	43 \pm 0.4
26	70.2 \pm 0.6	64 \pm 1.2	65.3 \pm 0.8	67.5 \pm 1.8	41.8 \pm 0.4	43.5 \pm 0.5
28	70.2 \pm 0.6	65.8 \pm 0.7	64.8 \pm 1.1	66 \pm 1.1	40.9 \pm 0.9	43.3 \pm 0.3
30	70.5 \pm 0.5	65.6 \pm 0.8	65.4 \pm 0.9	64.8 \pm 1.3	41.7 \pm 0.4	42.8 \pm 1
32	70.4 \pm 0.6	65.3 \pm 1.4	65.5 \pm 1	65.9 \pm 0.3	42.4 \pm 0.5	43.5 \pm 0.5
34	70.1 \pm 0.3	66.2 \pm 1.2	65.1 \pm 1.3	64.7 \pm 1.9	41.8 \pm 0.5	43.1 \pm 0.4
36	70.2 \pm 0.4	65.3 \pm 0.9	63.9 \pm 2.9	66.6 \pm 1.1	41.8 \pm 0.5	43.8 \pm 0.5
38	70.6 \pm 0.6	65.5 \pm 0.8	66.3 \pm 0.9	66.3 \pm 1.1	42 \pm 0.8	43.8 \pm 0.1
40	70.1 \pm 0.8	66.1 \pm 1.1	65.3 \pm 0.8	67.3 \pm 1.5	42 \pm 0.8	43.7 \pm 0.5
42	70.8 \pm 0.5	65.3 \pm 1.7	65.6 \pm 1.3	67.5 \pm 1.2	42.1 \pm 0.3	43.1 \pm 0.9
44	70.3 \pm 0.8	66.7 \pm 0.5	65 \pm 1.5	67.8 \pm 0.7	42.1 \pm 0.9	43.9 \pm 0.4
46	70.8 \pm 0.5	64.6 \pm 2.5	66.4 \pm 0.9	67 \pm 1.6	42.1 \pm 0.4	43.7 \pm 0.4
48	70.8 \pm 0.2	66.3 \pm 1.1	64.8 \pm 1	67.9 \pm 1	41.9 \pm 0.6	43.5 \pm 0.4
50	70.7 \pm 0.6	66.1 \pm 0.8	66.6 \pm 0.8	66 \pm 2.9	42.5 \pm 0.3	43.6 \pm 0.3

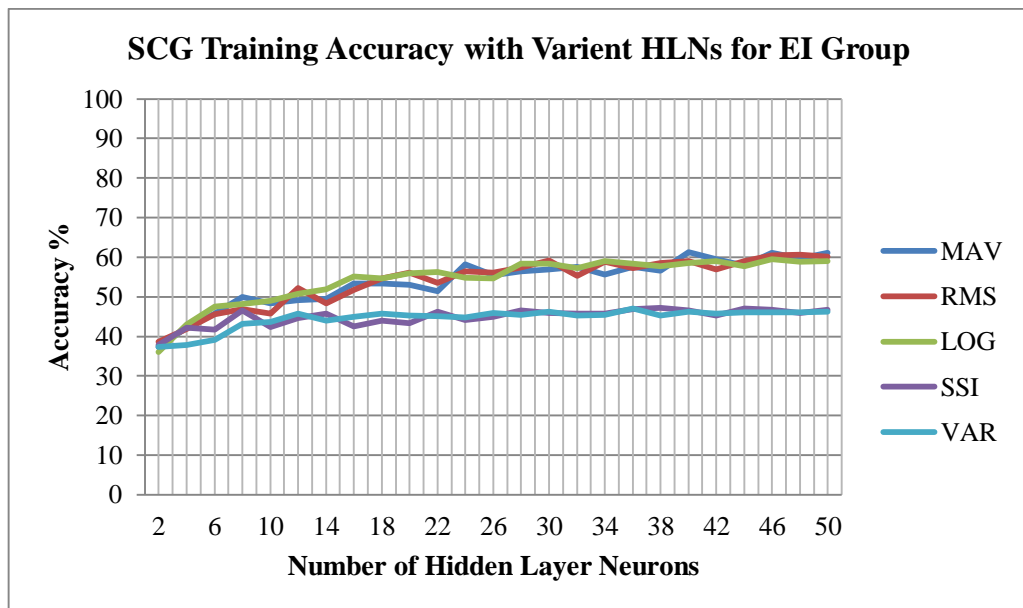


Figure 3.10 Accuracy rates of ANN training with SCG training function for EI group with variant hidden layer neurons

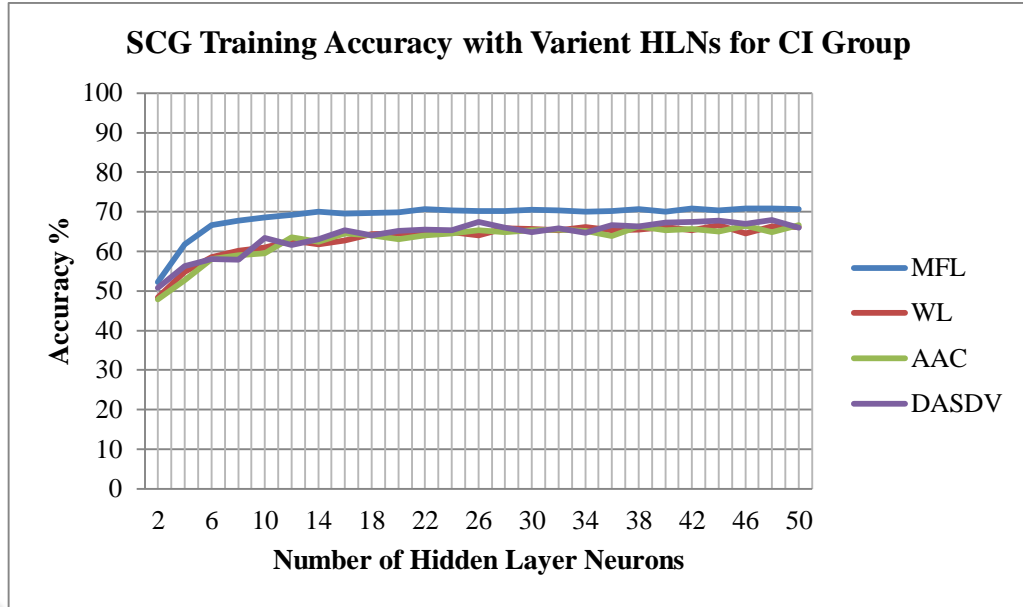


Figure 3.11 Accuracy rates of ANN training with SCG training function for the CI group with variant hidden layer neurons

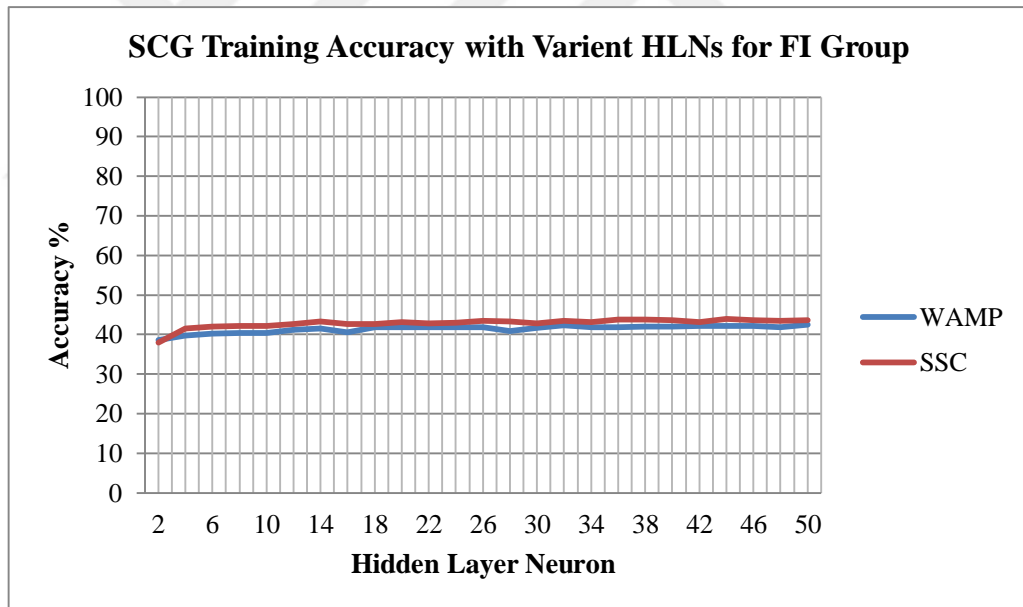


Figure 3.12 Accuracy rates of ANN training with SCG training function for FI group with variant hidden layer neurons

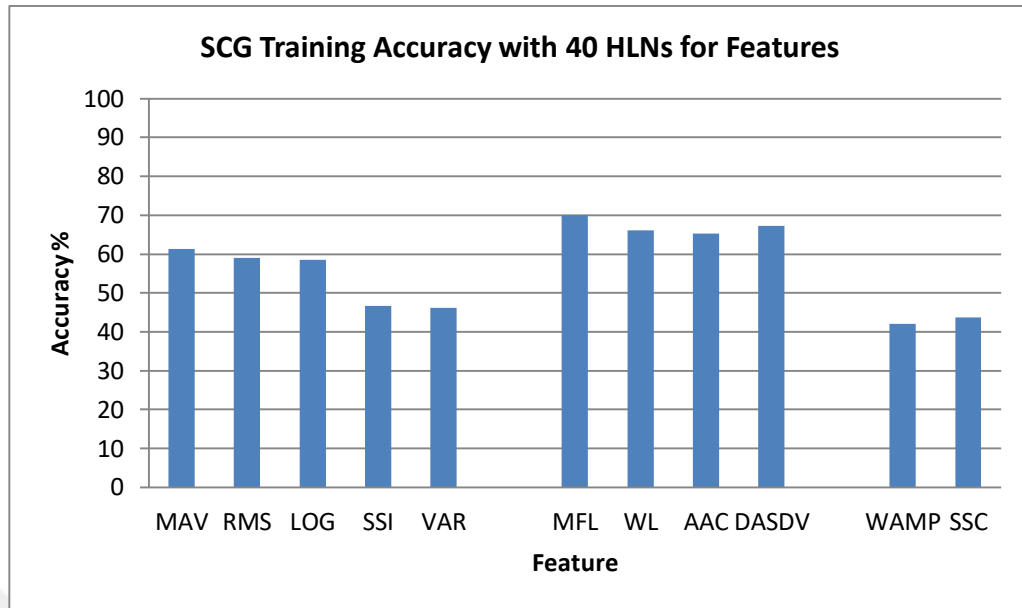
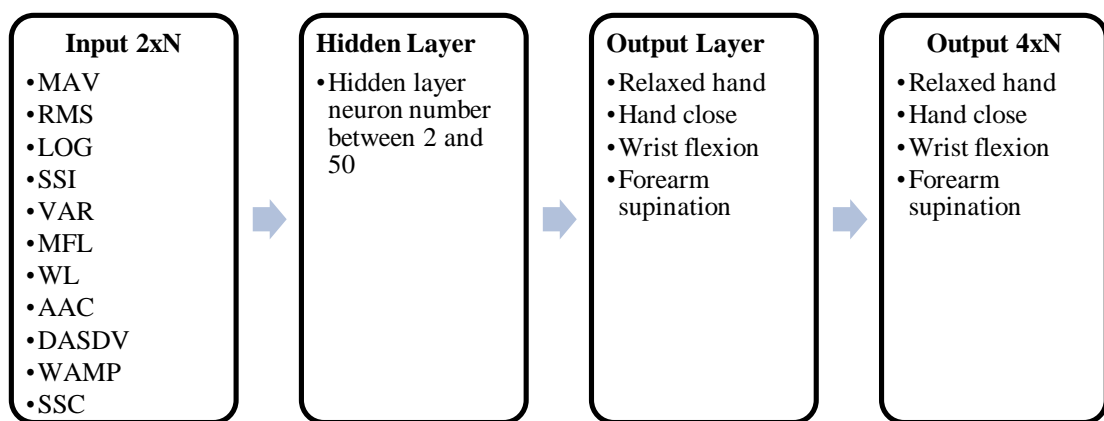


Figure 3.13 Accuracy rates of ANN training with SCG training function for 40 hidden layer neurons

The second trial conducted with Levenberg-Marquardt (LM) as training function and MSE as performance function. All features were tested with even numbers of hidden layer neurons between 30 and 50 (Figure 3.14). MAV feature from the EI group has given the best accuracy rate and followed by the RMS feature. MFL feature from the CI group has given the best accuracy rate and followed by the DASDV feature. SSC feature from the FI group has given the best accuracy (Table 3.6 & Table 3.7 & Figure 3.18).



Training Function: Levenberg-Marquardt

Input: 1 feature x 2 channel

Figure 3.14 Structure of ANN training with LM function

Table 3.6 Mean accuracy of 10 LM train trials for EI group

HLN	Accuracy \pm Std % - EI Group				
	MAV	RMS	LOG	SSI	VAR
2	36.8 \pm 2.9	39.7 \pm 2.3	37.1 \pm 2.9	37.5 \pm 2.1	36.8 \pm 2.7
4	36.8 \pm 2.3	39.7 \pm 2.7	37.1 \pm 2.4	37.5 \pm 2.2	36.8 \pm 3
6	46 \pm 2.3	45.7 \pm 2.1	48.1 \pm 2.4	41.1 \pm 2	39.2 \pm 2.7
8	46 \pm 2.6	45.7 \pm 2.9	48.1 \pm 2.4	41.1 \pm 3	39.2 \pm 2
10	48.7 \pm 2.1	45.4 \pm 2.7	49.6 \pm 2.8	43.3 \pm 2.7	44.4 \pm 2.5
12	48.7 \pm 2.6	45.4 \pm 3	49.6 \pm 2.7	43.3 \pm 2.3	44.4 \pm 2.8
14	50 \pm 2.7	47.3 \pm 2.8	52.3 \pm 2.3	45.2 \pm 2.3	43.1 \pm 2.1
16	50 \pm 2.2	47.3 \pm 2.5	52.3 \pm 3	45.2 \pm 2.6	43.1 \pm 2.8
18	53.7 \pm 2.3	55.2 \pm 2.5	55.1 \pm 2.7	44.9 \pm 2.1	45.2 \pm 2.7
20	53.7 \pm 2.9	55.2 \pm 2.1	55.1 \pm 2.2	44.9 \pm 2.3	45.2 \pm 2.3
22	51.5 \pm 2	54.5 \pm 2.3	56.8 \pm 2.7	45.5 \pm 2.3	44.8 \pm 2
24	51.5 \pm 2	54.5 \pm 2	56.8 \pm 2.7	45.5 \pm 2.2	44.8 \pm 3
26	54.9 \pm 2.6	57.1 \pm 2.9	53.6 \pm 2.1	45.7 \pm 2.4	46.8 \pm 2.8
28	54.9 \pm 2.5	57.1 \pm 2.6	53.6 \pm 2.8	45.7 \pm 2.2	46.8 \pm 3
30	57.4 \pm 2.2	60.1 \pm 2.8	57.9 \pm 3	46.7 \pm 2.7	46.4 \pm 3
32	57.5 \pm 5.2	55.3 \pm 3.9	57.2 \pm 2.6	45.7 \pm 1.6	45.2 \pm 1.7
34	55.7 \pm 5.1	58.9 \pm 2.4	59.1 \pm 0.6	45.8 \pm 1.7	45.4 \pm 0.5
36	57.5 \pm 2.5	57.2 \pm 2.5	58.3 \pm 1	46.9 \pm 1.2	47.1 \pm 1.8
38	56.6 \pm 5.6	58.5 \pm 4	57.7 \pm 2	47.2 \pm 1.7	45.3 \pm 1.3
40	61.3 \pm 1.1	59 \pm 2.8	58.6 \pm 0.8	46.6 \pm 1.3	46.2 \pm 1.2
42	59.5 \pm 1.8	56.9 \pm 1.6	59 \pm 1.1	45.3 \pm 1.3	45.8 \pm 3.4
44	57.9 \pm 5.3	59 \pm 0.8	57.8 \pm 2.3	47 \pm 1.3	46 \pm 2
46	61.1 \pm 2.1	60.4 \pm 1.1	59.5 \pm 1.2	46.8 \pm 2	46.1 \pm 1.3
48	59.6 \pm 4	60.6 \pm 3.2	58.9 \pm 1	45.9 \pm 1.2	46.1 \pm 2.3
50	61.1 \pm 1.4	60.1 \pm 3.7	59.1 \pm 1.3	46.8 \pm 1	46.3 \pm 1.6

Table 3.7 Mean accuracy of 10 LM train trials for CI Group and FI Group

HLN	Accuracy \pm Std % - CI Group				Accuracy \pm Std % - FI Group	
	MFL	WL	AAC	DASDV	WAMP	SSC
2	51.7 \pm 2.6	47.8 \pm 2.3	47.9 \pm 2	50.4 \pm 2.6	37.6 \pm 2.3	36.9 \pm 2.1
4	51.7 \pm 2.4	47.8 \pm 2.1	47.9 \pm 2	50.4 \pm 2.5	37.6 \pm 3	36.9 \pm 2.8
6	66.8 \pm 2.1	57.9 \pm 2.7	57.7 \pm 2.9	57.9 \pm 2.7	39.3 \pm 2.1	41 \pm 2.7
8	66.8 \pm 2.3	57.9 \pm 2.3	57.7 \pm 2.2	57.9 \pm 2	39.3 \pm 2.3	41 \pm 2.9
10	69.1 \pm 2.7	60.9 \pm 3	59.9 \pm 2.5	63.5 \pm 2.9	41.2 \pm 2.3	41.5 \pm 2.7
12	69.1 \pm 2.6	60.9 \pm 2.4	59.9 \pm 2.6	63.5 \pm 2.9	41.2 \pm 2.6	41.5 \pm 2.7
14	70.5 \pm 3	60.8 \pm 2.6	62.2 \pm 2.3	62.4 \pm 2.2	40.6 \pm 2	42.8 \pm 2.1
16	70.5 \pm 2.8	60.8 \pm 2.2	62.2 \pm 2.2	62.4 \pm 2.7	40.6 \pm 2.3	42.8 \pm 2.8
18	69.1 \pm 2.7	64.2 \pm 2.4	64 \pm 2.2	64.6 \pm 2.3	41.4 \pm 2.5	42.7 \pm 2.5
20	69.1 \pm 2.9	64.2 \pm 2	64 \pm 2.6	64.6 \pm 2	41.4 \pm 2.2	42.7 \pm 2
22	71.2 \pm 2.3	65 \pm 2.1	63.4 \pm 2.6	64.9 \pm 3	42.8 \pm 2.9	43.3 \pm 2.1
24	71.2 \pm 2.5	65 \pm 2.9	63.4 \pm 2.5	64.9 \pm 3	42.8 \pm 2.3	43.3 \pm 2.8
26	70 \pm 2.6	63.4 \pm 2.5	65.5 \pm 2.2	67.7 \pm 2.5	40.8 \pm 2.8	43.3 \pm 2.6
28	70 \pm 2.6	63.4 \pm 2.3	65.5 \pm 2.1	67.7 \pm 2.7	40.8 \pm 2.7	43.3 \pm 2
30	69.6 \pm 2.9	65.6 \pm 2.8	65.4 \pm 2.7	63.8 \pm 3	42.6 \pm 2.3	42.8 \pm 2.6
32	70.4 \pm 0.6	68 \pm 0.8	68.3 \pm 0.8	70.3 \pm 0.3	42.6 \pm 0.3	45.2 \pm 0.9
34	70.1 \pm 0.3	68.1 \pm 1	68.6 \pm 0.6	70.1 \pm 0.8	42.9 \pm 0.5	45.6 \pm 0.9
36	70.2 \pm 0.4	68.3 \pm 0.7	67.6 \pm 1.1	62.9 \pm 16.4	42.6 \pm 0.3	45.7 \pm 1.5
38	70.6 \pm 0.6	68.6 \pm 1.4	68.3 \pm 0.9	70.7 \pm 1.2	42.8 \pm 0.3	46 \pm 0.9
40	70.1 \pm 0.8	68.9 \pm 1.3	68.4 \pm 0.7	70.1 \pm 0.8	43 \pm 0.8	45.3 \pm 1.4
42	70.8 \pm 0.5	68.5 \pm 1.4	67.8 \pm 1	70.9 \pm 0.9	42 \pm 1.1	46.6 \pm 0.6
44	70.3 \pm 0.8	68 \pm 0.4	67.9 \pm 1.2	71.4 \pm 0.9	43.1 \pm 0.6	46.6 \pm 0.9
46	70.8 \pm 0.5	68 \pm 1.1	68.6 \pm 0.3	70.9 \pm 1.1	42.7 \pm 0.2	45.2 \pm 1
48	70.8 \pm 0.2	68.9 \pm 0.4	65.8 \pm 6	70.8 \pm 0.7	43.2 \pm 0.6	46.8 \pm 1.1
50	70.7 \pm 0.6	68.2 \pm 0.5	68.2 \pm 0.3	70.2 \pm 1.2	42.4 \pm 0.5	46.1 \pm 1.3

The effect of the hidden layer neuron number on accuracy was investigated separately for 3 feature groups. For EI group features, after the number of hidden layer neurons exceeded 40, no significant increase in accuracy was observed (Figure 3.15). Compared to the EI group, the increase in the number of hidden layer neurons had less effect on the CI group. After the number of neurons exceeded 10, there was no significant increase in accuracy (Figure 3.16). When the FI group was considered, an accuracy graph is obtained which is almost independent of the number of hidden layers. (Figure 3.17).

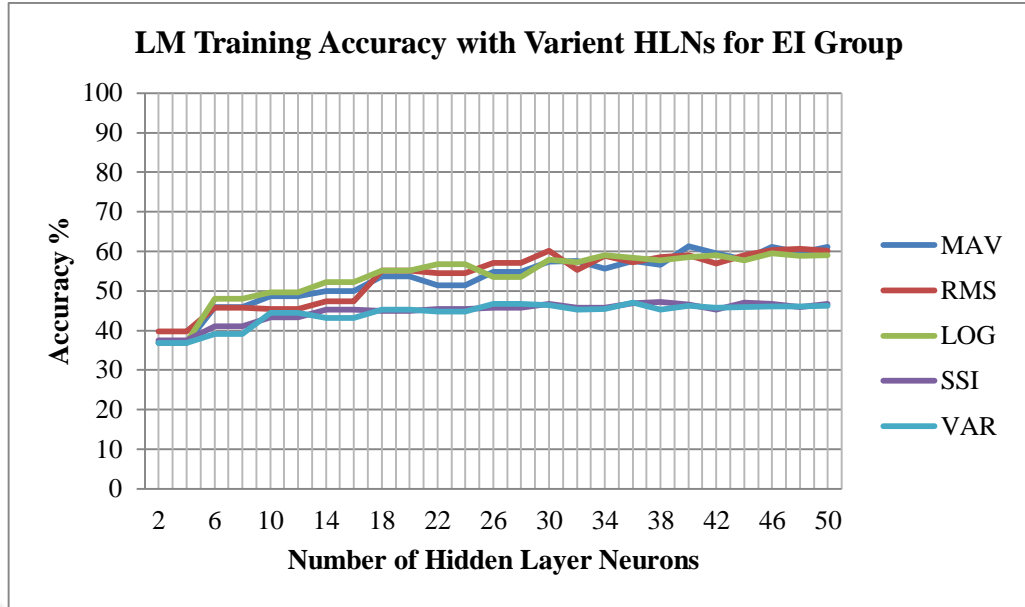


Figure 3.15 Accuracy rates of ANN training with LM training function for EI group with variant hidden layer neurons

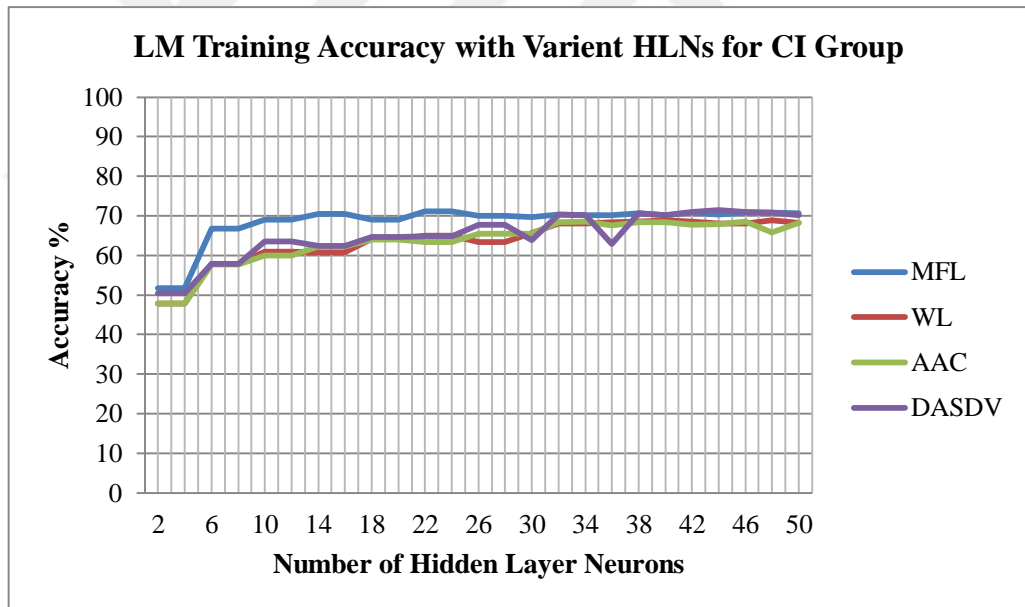


Figure 3.16 Accuracy rates of ANN training with LM training function for the CI group with variant hidden layer neurons

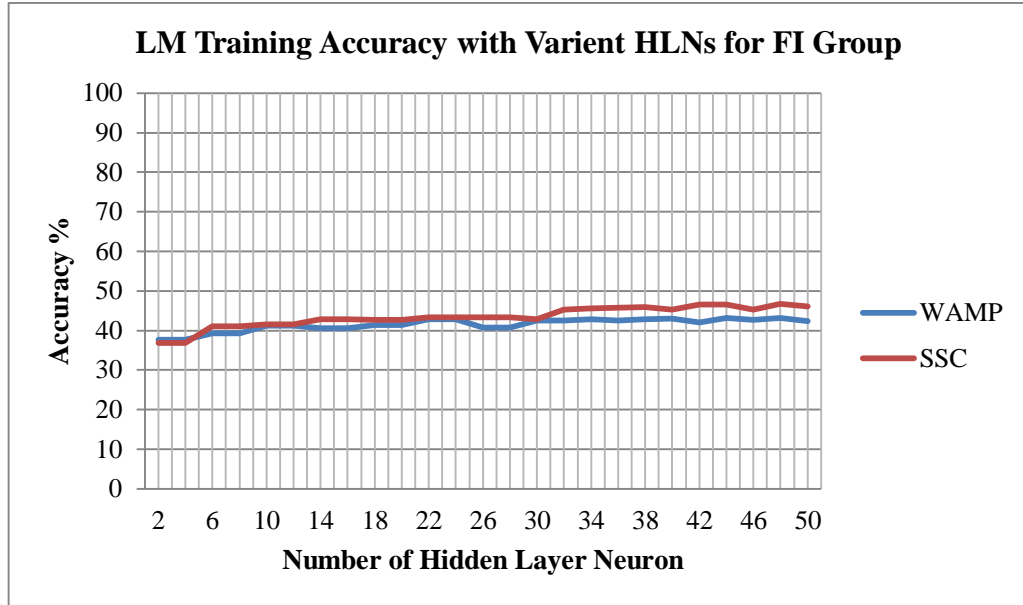


Figure 3.17 Accuracy rates of ANN training with LM training function for FI group with variant hidden layer neurons

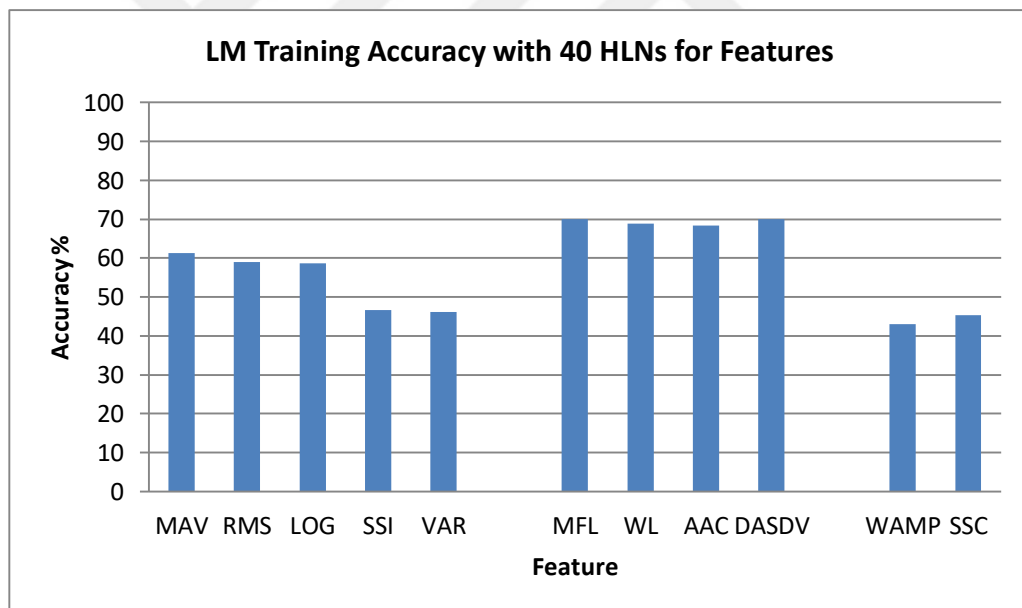
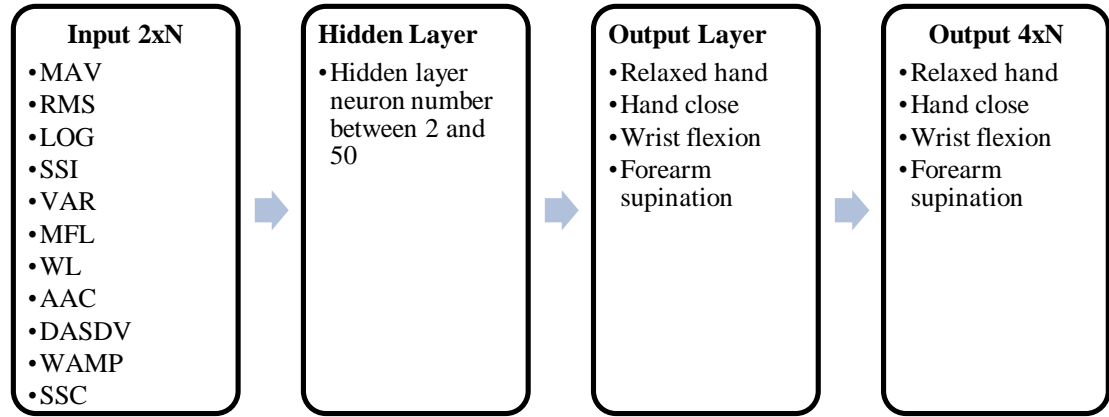


Figure 3.18 Accuracy rates of ANN training with LM training function for 40 hidden layer neurons

The third trial conducted with Bayesian Regression (BR) as training function and MSE as performance function. All features were tested with even numbers of hidden layer neurons between 30 and 50 (Figure 3.19). RMS feature from the EI group has given the best accuracy rate and followed by the MAV feature. MFL feature from the

CI group has given the best accuracy rate and followed by DASDV. SSC feature from the FI group has given the best accuracy (Table 3.8 & Table 3.9 & Figure 3.23).



Training Function: Bayesian Regression

Input: 1 feature x 2 channel

Figure 3.19 Structure of ANN training with BR function

Table 3.8 Mean accuracy of 10 BR train trials for EI group

HLN	Accuracy \pm Std % - EI Group				
	MAV	RMS	LOG	SSI	VAR
2	38 \pm 2.3	38 \pm 2.6	37.1 \pm 2.5	36.8 \pm 2.9	36.7 \pm 2.6
4	38 \pm 2.4	38 \pm 2.7	37.1 \pm 2.2	36.8 \pm 3	36.7 \pm 2.1
6	45.7 \pm 2.9	46.2 \pm 2.3	48.5 \pm 2	42.2 \pm 2.1	38.5 \pm 2.4
8	45.7 \pm 2.8	46.2 \pm 2.9	48.5 \pm 2.5	42.2 \pm 2.1	38.5 \pm 2
10	47.5 \pm 2	45.9 \pm 2.3	49.5 \pm 2	41.3 \pm 2.8	44.3 \pm 2.6
12	47.5 \pm 2.1	45.9 \pm 3	49.5 \pm 2.9	41.3 \pm 2.5	44.3 \pm 3
14	50 \pm 2.4	48 \pm 2.2	52.1 \pm 2.8	46.7 \pm 2	43.6 \pm 2.2
16	50 \pm 2.9	48 \pm 2	52.1 \pm 2.5	46.7 \pm 2.7	43.6 \pm 2.3
18	53.1 \pm 2	54.4 \pm 2.6	55.6 \pm 2	44.3 \pm 2.4	45 \pm 2.5
20	53.1 \pm 2.7	54.4 \pm 2.6	55.6 \pm 2	44.3 \pm 2.5	45 \pm 2.3
22	52.2 \pm 2.8	54.3 \pm 2	56.2 \pm 2.6	46.7 \pm 2.5	44.7 \pm 2.1
24	52.2 \pm 3	54.3 \pm 2.4	56.2 \pm 2.7	46.7 \pm 2.3	44.7 \pm 2.4
26	56.4 \pm 2.9	56.6 \pm 2.4	54.7 \pm 2.1	45.9 \pm 2.1	46.5 \pm 2.4
28	56.4 \pm 2	56.6 \pm 2.3	54.7 \pm 2.3	45.9 \pm 2.9	46.5 \pm 2.2
30	65.3 \pm 0.7	66.8 \pm 1.1	58.1 \pm 11	62.6 \pm 7.2	59.5 \pm 9.9
32	65.3 \pm 0.7	66.8 \pm 1.1	58.1 \pm 11	62.6 \pm 7.2	59.5 \pm 9.9
34	64.9 \pm 1.1	66 \pm 0.8	64.2 \pm 1.1	66.5 \pm 0.8	58.6 \pm 15.8
36	65.8 \pm 0.6	66.4 \pm 1.4	63.7 \pm 5.3	65.6 \pm 1.8	58.4 \pm 14.2
38	66.2 \pm 0.8	67 \pm 1	63.8 \pm 1.4	65.9 \pm 1.7	62.9 \pm 3.5
40	65.1 \pm 1.2	66.6 \pm 0.8	61.2 \pm 6.7	57.9 \pm 12.7	66.5 \pm 1.1
42	62.2 \pm 6.9	65.6 \pm 1.7	62.9 \pm 2	61.1 \pm 9.8	66.2 \pm 1.5
44	66 \pm 0.5	67 \pm 1.6	62.8 \pm 1.5	56.2 \pm 17.7	57.7 \pm 1.7
46	66.2 \pm 1.1	67.4 \pm 0.7	64.9 \pm 1.4	64.5 \pm 2.6	62.4 \pm 1.2
48	65.9 \pm 0.4	67.6 \pm 0.6	64.6 \pm 1.5	61.9 \pm 6.3	67.1 \pm 0.9
50	66.3 \pm 0.3	65.5 \pm 3.4	63.6 \pm 1.7	60.6 \pm 7.8	62 \pm 6.2

The effect of the hidden layer neuron number on accuracy was investigated separately for 3 feature groups. For group 1 features, after the number of hidden layer neurons exceeded 40, no significant increase in accuracy was observed (Figure 3.20). Compared to feature group 1, the increase in the number of hidden layer neurons had less effect on feature group 2. After the number of neurons exceeded 10, there was no significant increase in accuracy (Figure 3.21). When feature group 3 was considered, an accuracy graph is obtained which is almost independent of the number of hidden layers. (Figure 3.22).

Table 3.9 Mean accuracy of 10 BR train trials for the CI group and FI group

HLN	Accuracy \pm Std % - CI Group			Accuracy \pm Std % - FI Group		
	MFL	WL	AAC	DASDV	WAMP	SSC
2	53.2 \pm 2.5	48.7 \pm 2.5	47 \pm 2.2	51.7 \pm 2.5	37.7 \pm 2.7	38.8 \pm 3
4	53.2 \pm 2	48.7 \pm 2.2	47 \pm 2.6	51.7 \pm 2.8	37.7 \pm 2.6	38.8 \pm 2.3
6	67.6 \pm 2.6	58.8 \pm 2	57.4 \pm 2.3	58.5 \pm 2.9	40.9 \pm 2.4	42.1 \pm 3
8	67.6 \pm 3	58.8 \pm 2.3	57.4 \pm 2.4	58.5 \pm 2.7	40.9 \pm 2.7	42.1 \pm 2.8
10	69.1 \pm 2.6	61.8 \pm 2.3	60 \pm 2.2	64.1 \pm 3	40.2 \pm 3	42.1 \pm 2.6
12	69.1 \pm 2.1	61.8 \pm 3	60 \pm 2	64.1 \pm 2.5	40.2 \pm 2	42.1 \pm 2.9
14	69.8 \pm 2.5	61.7 \pm 2.7	63.5 \pm 2	63.6 \pm 2.5	42.5 \pm 2.8	42.5 \pm 2.9
16	69.8 \pm 2.1	61.7 \pm 2.6	63.5 \pm 2.1	63.6 \pm 3	42.5 \pm 2.1	42.5 \pm 2.9
18	68.7 \pm 2.8	64.5 \pm 2.5	64.1 \pm 2.8	65.1 \pm 2.5	42.5 \pm 2.4	41.7 \pm 3
20	68.7 \pm 2.9	64.5 \pm 2.7	64.1 \pm 2.4	65.1 \pm 3	42.5 \pm 2.8	41.7 \pm 2.7
22	70.7 \pm 2.9	65.4 \pm 2.3	63.6 \pm 2.4	66.4 \pm 2.3	41.1 \pm 2.8	42.3 \pm 2.6
24	70.7 \pm 2.9	65.4 \pm 2	63.6 \pm 2.6	66.4 \pm 3	41.1 \pm 2.1	42.3 \pm 2.5
26	70.5 \pm 3	64 \pm 2.4	65.9 \pm 2.7	68.5 \pm 2.4	42.6 \pm 2.9	43.6 \pm 2.9
28	70.5 \pm 2.3	64 \pm 2.8	65.9 \pm 2.7	68.5 \pm 2.2	42.6 \pm 2.4	43.6 \pm 3
30	68.8 \pm 4.8	66.8 \pm 1.4	67.2 \pm 0.7	70.8 \pm 0.6	41.1 \pm 1.2	44.3 \pm 2
32	69.2 \pm 4.8	68.7 \pm 1.3	68.3 \pm 0.8	71.2 \pm 0.6	42.9 \pm 0.2	45.9 \pm 1
34	69.5 \pm 4.9	65 \pm 7.8	67.8 \pm 0.8	68.6 \pm 6.2	42.5 \pm 1.2	45.6 \pm 1.6
36	71.5 \pm 0.4	68 \pm 0.7	65.3 \pm 8	71.1 \pm 1.2	42.3 \pm 1.1	43.8 \pm 1.7
38	71.2 \pm 0.4	68.8 \pm 0.7	65.3 \pm 5.9	70.7 \pm 0.9	43.1 \pm 0.3	44.9 \pm 1.5
40	71.5 \pm 0.5	67.8 \pm 1.5	68.1 \pm 0.7	71.1 \pm 0.6	43.2 \pm 0.3	46 \pm 1.8
42	68.5 \pm 6.9	68.5 \pm 1.3	67.9 \pm 0.9	70 \pm 0.3	42.2 \pm 1.2	46.3 \pm 1.1
44	71.4 \pm 0.6	67.9 \pm 0.6	68.5 \pm 0.9	71.3 \pm 0.6	43.3 \pm 0.5	45.1 \pm 2.8
46	72 \pm 0.6	67.9 \pm 1.4	63.2 \pm 12.7	65.8 \pm 11.9	43.1 \pm 0.2	45.5 \pm 1.6
48	66.5 \pm 7.1	68.8 \pm 0.7	68.2 \pm 0.6	66.6 \pm 8.4	42.1 \pm 1.8	44.8 \pm 2
50	68.5 \pm 6.9	67.8 \pm 1.1	67.8 \pm 1	71 \pm 0.5	42.2 \pm 1.9	45.8 \pm 3

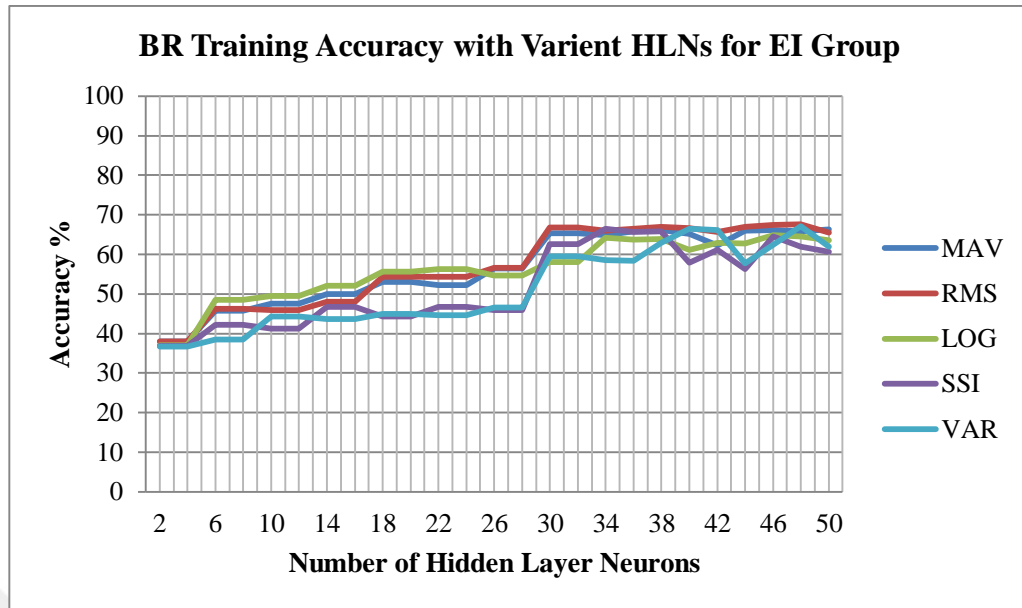


Figure 3.20 Accuracy rates of ANN training with BR training function for EI group with variant hidden layer neurons

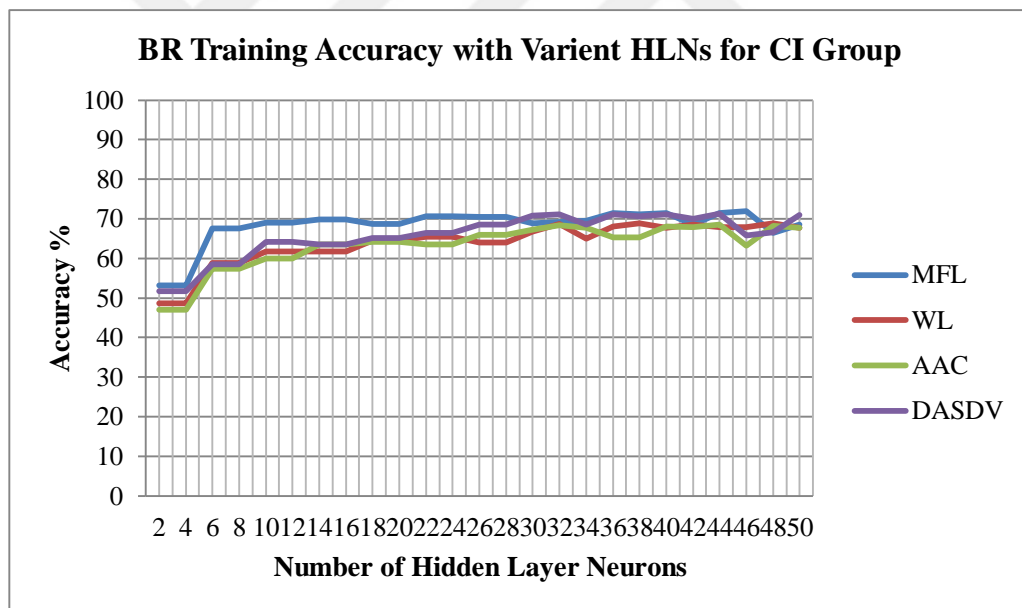


Figure 3.21 Accuracy rates of ANN training with BR training function for CI group with variant hidden layer neurons

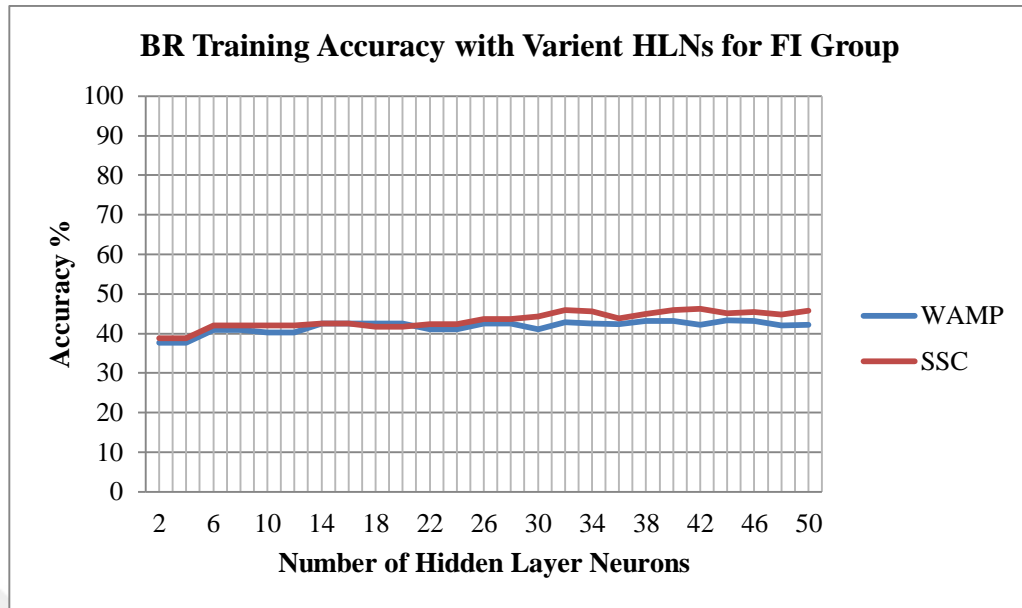


Figure 3.22 Accuracy rates of ANN training with BR training function for FI group with variant hidden layer neurons

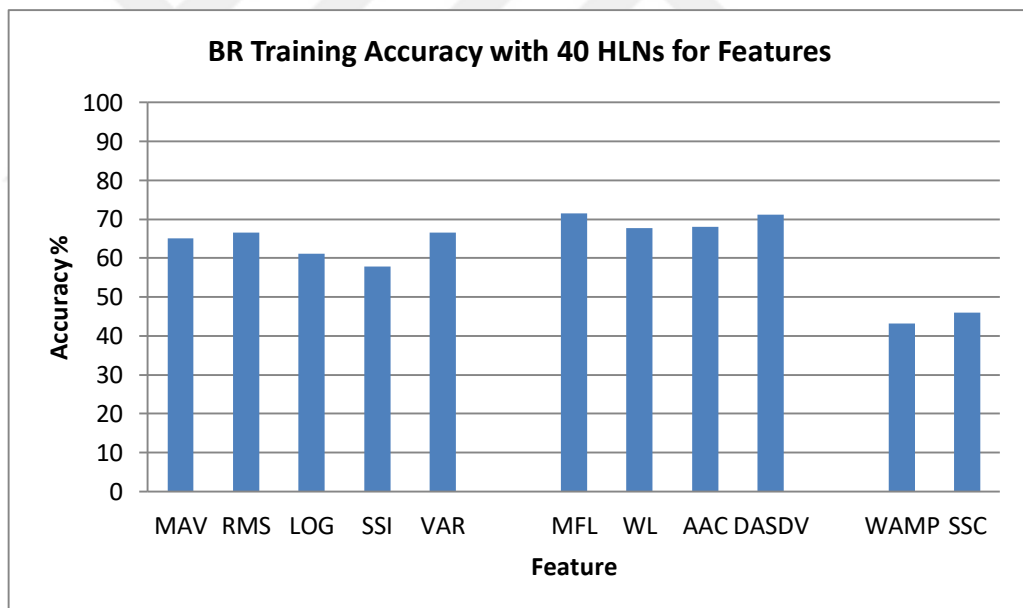


Figure 3.23 Accuracy rates of ANN training with BR training function for 40 hidden layer neurons

For further tests to build optimal ANN structure two different feature sets are determined as MFL, MAV, DASDV, AAC and SSC for Set 1, MFL, RMS, DASDV, AAC and SSC for Set 2. Both feature sets are tested with SCG, LM and BR train functions with even hidden layer neuron numbers between 2 and 50.

Subsequently, these feature sets were used in the training of user-specific ANN structures. In this way, the accuracy rates of ANNs trained in generalized and user-specific training were evaluated.

Effect of feature groups evaluated by excluding feature groups one by one. When the number of hidden layer neurons was selected between 30 and 50, close values were obtained for accuracy. Therefore, for evaluating the effects of feature groups on ANN accuracy is tested with 40 hidden layer neurons, which is an average of 30 and 50.



CHAPTER FOUR

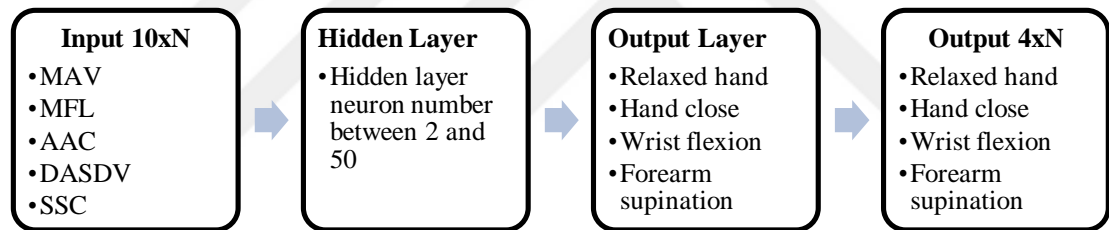
RESULTS

In this chapter, the classification performance of previously determined feature sets, and generalized and individualized classification approaches are evaluated. Finally, the effects of the exclusion of features are evaluated.

4.1 Classification

4.1.1 Feature Set 1

ANN was trained with the SCG, LM and BR training function using the feature set 1 as an input vector. The number of hidden layer nodes is selected between 2 and 50 (Figure 4.1). ANN training gave the best results when the number of hidden layer neurons was between 30 and 50 (Figure 4.2). When SCG was used as a training function, the accuracy rate decreased significantly.



Training Function: Scaled Conjugate Gradient, Levenberg-Marquardt and Bayesian Regression

Input: 5 feature x 2 channel

Figure 4.1 Structure of ANN training with SCG, LM and BR functions for the feature set 1

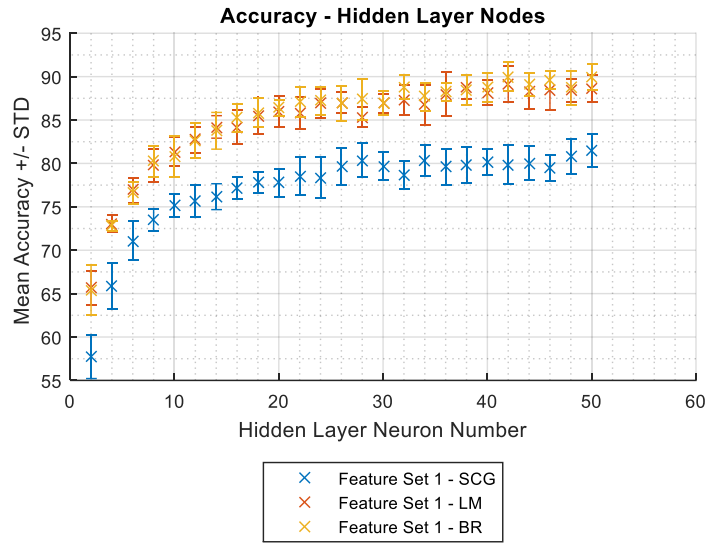


Figure 4.2 Mean accuracy of ANN with Set 1 and the variant number of hidden layer neurons

Sensitivity value was calculated from highest to lowest as the relaxed hand (C1), wrist flexion (C3), forearm supination (C4) and hand close (C2) for a number of hidden layer neurons between 30 and 50 in Table 4.1.

Specificity and precision values were calculated from highest to lowest as C1, wrist flexion C3, hand close C2 and forearm supination C4 for a number of hidden layer neurons between 30 and 50 (Table 4.2 & Table 4.3).

Table 4.1 Sensitivity of ANN training with Set 1

HLN	Set 1 - SCG				Set 1 - LM				Set 1 - BR			
	C1	C2	C3	C4	C1	C2	C3	C4	C1	C2	C3	C4
30	0.82	0.64	0.73	0.70	0.86	0.74	0.79	0.78	0.86	0.74	0.79	0.78
32	0.81	0.62	0.74	0.70	0.87	0.75	0.81	0.79	0.87	0.75	0.81	0.79
34	0.82	0.65	0.74	0.72	0.87	0.75	0.79	0.79	0.87	0.75	0.79	0.79
36	0.82	0.63	0.73	0.71	0.88	0.74	0.80	0.79	0.88	0.74	0.80	0.79
38	0.82	0.64	0.73	0.71	0.87	0.75	0.80	0.79	0.87	0.75	0.80	0.79
40	0.82	0.65	0.74	0.71	0.87	0.76	0.81	0.79	0.87	0.76	0.81	0.79
42	0.82	0.63	0.74	0.71	0.88	0.77	0.82	0.81	0.88	0.77	0.82	0.81
44	0.82	0.65	0.74	0.70	0.87	0.77	0.81	0.79	0.87	0.77	0.81	0.79
46	0.81	0.64	0.74	0.70	0.88	0.77	0.81	0.80	0.88	0.77	0.81	0.80
48	0.82	0.65	0.75	0.72	0.87	0.76	0.81	0.79	0.87	0.76	0.81	0.79
50	0.82	0.67	0.75	0.72	0.87	0.77	0.82	0.80	0.87	0.77	0.82	0.80

Table 4.2 Specificity of ANN training with Set 1

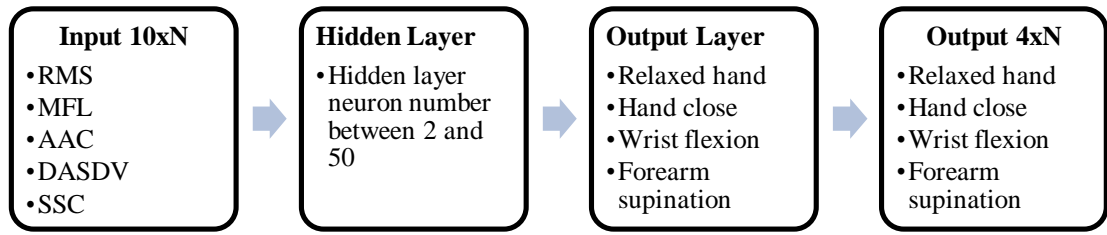
HLN	Set 1 - SCG				Set 1 - LM				Set 1 - BR			
	C1	C2	C3	C4	C1	C2	C3	C4	C1	C2	C3	C4
30	0.87	0.84	0.86	0.82	0.89	0.87	0.87	0.85	0.89	0.87	0.88	0.85
32	0.87	0.84	0.85	0.81	0.89	0.87	0.88	0.85	0.89	0.88	0.88	0.85
34	0.87	0.85	0.86	0.82	0.88	0.87	0.87	0.85	0.89	0.87	0.88	0.85
36	0.87	0.85	0.86	0.82	0.89	0.87	0.88	0.86	0.89	0.88	0.88	0.85
38	0.87	0.84	0.86	0.82	0.89	0.87	0.88	0.85	0.89	0.87	0.88	0.85
40	0.87	0.85	0.86	0.82	0.89	0.87	0.88	0.86	0.89	0.88	0.88	0.86
42	0.87	0.85	0.86	0.82	0.89	0.88	0.88	0.86	0.89	0.88	0.88	0.86
44	0.87	0.85	0.86	0.82	0.89	0.87	0.88	0.86	0.89	0.88	0.88	0.86
46	0.87	0.85	0.85	0.82	0.89	0.87	0.88	0.86	0.89	0.88	0.88	0.86
48	0.87	0.85	0.86	0.82	0.89	0.88	0.88	0.85	0.89	0.88	0.88	0.85
50	0.87	0.85	0.86	0.83	0.89	0.87	0.88	0.86	0.89	0.88	0.88	0.86

Table 4.3 Precision of ANN training with Set 1

HLN	Set 1 - SCG				Set 1 - LM				Set 1 - BR			
	C1	C2	C3	C4	C1	C2	C3	C4	C1	C2	C3	C4
30	0.79	0.70	0.75	0.66	0.84	0.78	0.80	0.74	0.84	0.78	0.81	0.74
32	0.80	0.68	0.74	0.64	0.84	0.78	0.81	0.74	0.85	0.81	0.82	0.75
34	0.80	0.71	0.75	0.67	0.84	0.79	0.80	0.73	0.85	0.79	0.81	0.74
36	0.79	0.70	0.75	0.66	0.85	0.79	0.81	0.75	0.85	0.80	0.82	0.75
38	0.79	0.70	0.75	0.66	0.85	0.80	0.83	0.75	0.85	0.79	0.82	0.75
40	0.79	0.70	0.76	0.67	0.85	0.79	0.81	0.75	0.85	0.80	0.82	0.75
42	0.79	0.71	0.75	0.66	0.85	0.81	0.82	0.77	0.86	0.81	0.83	0.77
44	0.79	0.70	0.75	0.66	0.85	0.79	0.82	0.76	0.85	0.80	0.82	0.76
46	0.80	0.70	0.74	0.66	0.85	0.80	0.82	0.76	0.86	0.81	0.83	0.76
48	0.80	0.72	0.76	0.67	0.84	0.80	0.82	0.75	0.85	0.80	0.82	0.75
50	0.80	0.72	0.76	0.68	0.85	0.80	0.82	0.76	0.86	0.81	0.83	0.77

4.1.2 Feature Set 2

ANN was trained with the SCG, LM and BR training function using the feature set 2 as an input vector (Figure 4.3). The number of hidden layer neurons is selected between 2 and 50 (Figure 4.4). ANN training gave the best results when the number of hidden layer neurons was between 30 and 50 (Figure 4.4). When SCG was used as a training function, the accuracy rate decreased significantly.



Training Function: Scaled Conjugate Gradient, Levenberg-Marquardt and Bayesian Regression

Input: 5 feature x 2 channel

Figure 4.3 Structure of ANN training with SCG, LM and BR functions for the feature set 2

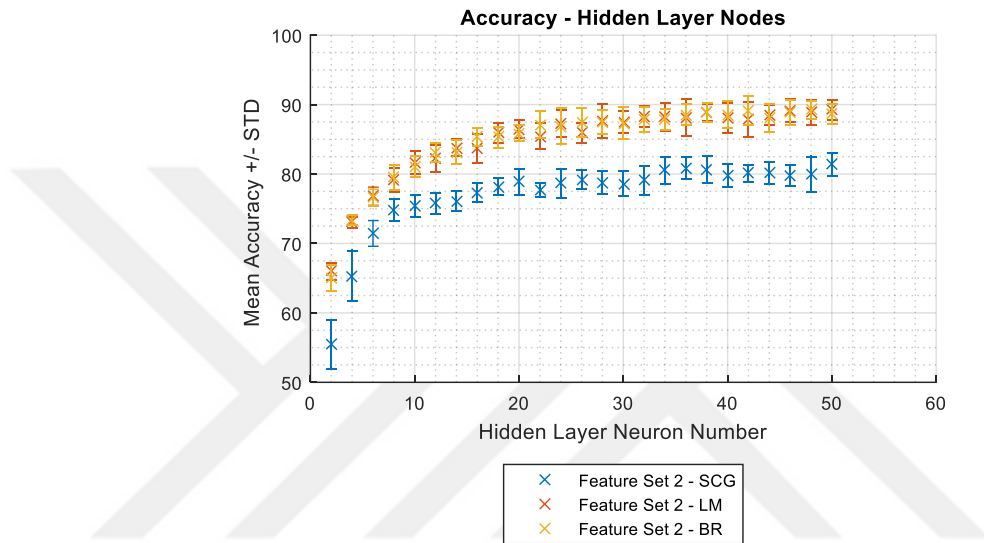


Figure 4.4 Mean accuracy of ANN with Set 2 and variant number of hidden layer neurons

Sensitivity value was calculated from highest to lowest as C1, C3, C4 and C2 for a number of hidden layer neurons between 30 and 50 (Table 4.4).

Specificity and precision values were calculated from highest to lowest as C1, C3, C2 and forearm supination C4 for a number of hidden layer neurons between 30 and 50 (Table 4.5 & Table 4.6).

Table 4.4 Sensitivity of ANN training with Set 2

HLN	Set 2 - SCG				Set 2 - LM				Set 2 - BR			
	C1	C2	C3	C4	C1	C2	C3	C4	C1	C2	C3	C4
	SCG				LM				BR			
30	0.80	0.63	0.72	0.70	0.87	0.74	0.79	0.78	0.86	0.73	0.80	0.78
32	0.81	0.63	0.72	0.70	0.87	0.74	0.80	0.79	0.87	0.74	0.80	0.79
34	0.82	0.66	0.74	0.71	0.86	0.74	0.81	0.79	0.86	0.74	0.80	0.79
36	0.81	0.65	0.75	0.72	0.87	0.75	0.80	0.79	0.87	0.75	0.80	0.79
38	0.82	0.65	0.74	0.72	0.87	0.75	0.81	0.79	0.87	0.75	0.82	0.79
40	0.81	0.64	0.73	0.72	0.87	0.74	0.80	0.79	0.87	0.75	0.81	0.79
42	0.82	0.64	0.74	0.72	0.87	0.74	0.80	0.79	0.87	0.76	0.82	0.80
44	0.82	0.64	0.74	0.71	0.86	0.75	0.81	0.80	0.87	0.75	0.81	0.78
46	0.82	0.63	0.73	0.72	0.87	0.76	0.81	0.80	0.87	0.76	0.81	0.80
48	0.82	0.64	0.73	0.71	0.87	0.75	0.81	0.79	0.87	0.76	0.81	0.80
50	0.82	0.66	0.75	0.72	0.87	0.76	0.81	0.80	0.87	0.75	0.81	0.79

Table 4.5 Specificity of ANN training with Set 2

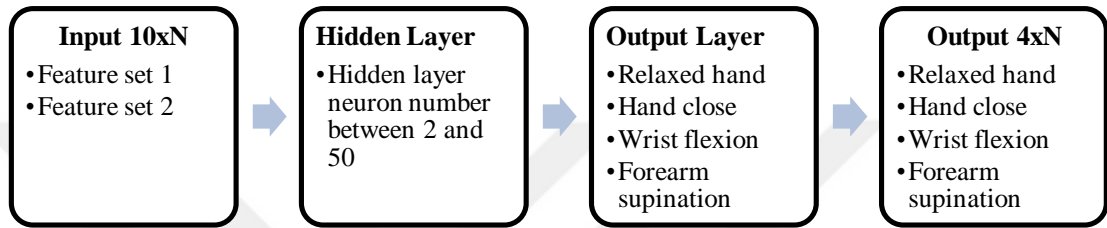
HLN	Set 2 - SCG				Set 2 - LM				Set 2 - BR			
	C1	C2	C3	C4	C1	C2	C3	C4	C1	C2	C3	C4
30	0.87	0.84	0.85	0.81	0.88	0.87	0.88	0.85	0.88	0.87	0.88	0.85
32	0.87	0.84	0.86	0.82	0.89	0.87	0.88	0.85	0.89	0.87	0.88	0.85
34	0.87	0.85	0.86	0.82	0.89	0.87	0.88	0.85	0.89	0.87	0.88	0.85
36	0.87	0.85	0.86	0.82	0.89	0.87	0.88	0.85	0.89	0.87	0.88	0.85
38	0.87	0.85	0.86	0.82	0.89	0.88	0.88	0.86	0.89	0.88	0.88	0.86
40	0.87	0.85	0.86	0.82	0.89	0.87	0.88	0.85	0.89	0.87	0.88	0.85
42	0.87	0.85	0.86	0.82	0.89	0.87	0.88	0.85	0.89	0.88	0.88	0.86
44	0.87	0.85	0.86	0.82	0.89	0.87	0.88	0.85	0.89	0.87	0.88	0.85
46	0.87	0.85	0.86	0.82	0.89	0.88	0.88	0.86	0.89	0.88	0.88	0.85
48	0.87	0.85	0.86	0.82	0.89	0.88	0.88	0.86	0.89	0.88	0.88	0.86
50	0.87	0.85	0.86	0.83	0.89	0.88	0.88	0.86	0.89	0.88	0.88	0.85

Table 4.6 Precision of ANN training with Set 2

HLN	Set 2 - SCG				Set 2 - LM				Set 2 - BR			
	C1	C2	C3	C4	C1	C2	C3	C4	C1	C2	C3	C4
30	0.79	0.68	0.74	0.65	0.84	0.78	0.82	0.74	0.84	0.79	0.81	0.74
32	0.79	0.69	0.75	0.65	0.85	0.80	0.82	0.75	0.84	0.79	0.82	0.75
34	0.80	0.71	0.75	0.66	0.85	0.79	0.82	0.75	0.84	0.80	0.81	0.74
36	0.80	0.72	0.76	0.67	0.85	0.79	0.81	0.75	0.85	0.80	0.82	0.75
38	0.80	0.71	0.76	0.67	0.85	0.80	0.82	0.76	0.86	0.81	0.81	0.76
40	0.79	0.70	0.75	0.66	0.85	0.79	0.81	0.75	0.86	0.80	0.82	0.75
42	0.79	0.71	0.76	0.67	0.85	0.79	0.82	0.74	0.86	0.80	0.82	0.76
44	0.79	0.71	0.75	0.66	0.85	0.80	0.82	0.75	0.85	0.80	0.81	0.75
46	0.79	0.71	0.75	0.66	0.86	0.80	0.83	0.76	0.85	0.80	0.83	0.76
48	0.79	0.71	0.75	0.66	0.85	0.81	0.82	0.76	0.85	0.81	0.83	0.76
50	0.80	0.72	0.76	0.68	0.86	0.81	0.82	0.76	0.85	0.80	0.82	0.75

4.1.3 Generalized and Individualized Classification

ANN was trained 10 times with data from all subjects, and the mean accuracy and standard deviation were calculated (Figure 4.5). A maximum success rate for accuracy calculated as 90% (Table 4.7) using the feature set 1 as input, BR as training function and 42 hidden layer neurons. In the performance plot of generalized ANN, the best validation performance is obtained at epoch 44 (Figure 4.6). However, after 24th epoch, validation and test errors were stable.



Training Function: Scaled Conjugate Gradient, Levenberg-Marquardt and Bayesian Regression
Input: 5 feature x 2 channel

Figure 4.5 Structure of generalized ANN training with SCG, LM and BR functions for the feature set 1

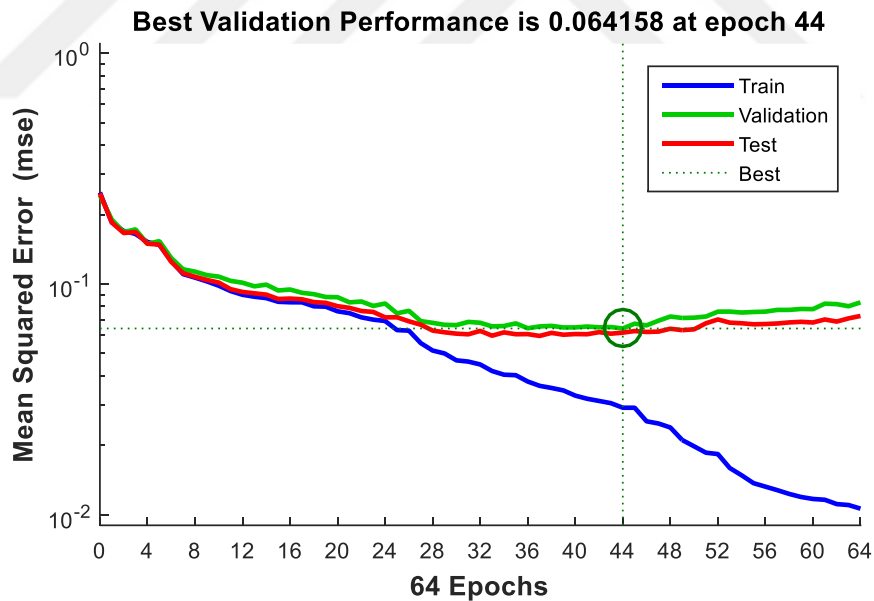
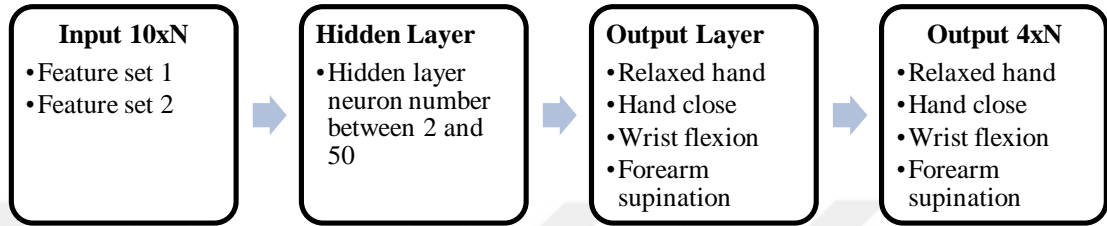


Figure 4.6 Performance plot of generalized ANN training

Table 4.7 Accuracy rates of generalized ANN

HLN	Set 1 - SCG		Set 1 - LM		Set 1 - BR		Set 2 - SCG		Set 2 - LM		Set 2 - BR	
	Mean	\pm Std	Mean	\pm Std	Mean	\pm Std	Mean	\pm Std	Mean	\pm Std	Mean	\pm Std
2	57.7	2.5	65.7	2.0	65.4	2.9	55.4	3.6	66.0	1.2	65.0	1.9
4	65.8	2.6	73.1	1.0	72.8	0.6	65.3	3.6	73.0	0.8	73.4	0.7
6	71.1	2.2	76.9	1.4	76.6	1.2	71.4	1.9	76.8	1.3	76.6	1.2
8	73.5	1.3	79.8	1.9	80.2	1.8	74.8	1.6	79.1	1.8	79.5	1.8
10	75.2	1.3	81.4	1.7	80.8	2.4	75.4	1.6	81.6	1.6	81.1	1.6
12	75.6	1.8	82.7	1.5	82.7	2.0	75.7	1.5	82.2	1.9	83.1	1.4
14	76.2	1.5	84.2	1.3	83.8	2.1	76.1	1.4	83.8	1.2	83.2	1.7
16	77.2	1.3	84.2	1.9	85.2	1.6	77.4	1.3	83.7	2.1	85.4	1.3
18	77.8	1.2	85.5	2.1	85.8	1.7	78.2	1.2	85.9	1.4	85.3	1.5
20	77.8	1.6	85.9	1.8	86.4	1.0	78.9	1.9	86.4	1.3	85.9	1.1
22	78.5	2.2	85.8	1.9	87.1	1.8	77.7	1.0	85.5	1.9	87.1	2.0
24	78.4	2.4	86.9	1.7	87.2	1.6	78.6	2.1	87.3	2.0	86.9	2.6
26	79.7	2.1	87.0	1.2	86.9	2.0	79.2	1.4	85.9	1.4	87.4	2.1
28	80.4	1.9	85.3	1.1	87.4	2.4	78.8	1.6	87.6	2.5	87.5	1.7
30	79.7	1.6	86.9	1.1	87.0	1.4	78.6	1.8	87.5	1.5	87.3	2.3
32	78.7	1.6	87.3	1.8	88.8	1.4	79.1	2.1	88.2	1.5	87.8	1.8
34	80.3	1.8	86.7	2.3	87.7	1.6	80.5	2.0	88.2	2.1	87.8	1.5
36	79.6	2.1	88.0	2.5	88.2	1.1	80.8	1.6	88.1	2.6	88.6	1.5
38	79.8	2.1	88.8	1.4	88.4	1.7	80.7	1.9	88.9	1.2	88.9	1.4
40	80.1	1.5	88.2	1.4	88.7	1.6	79.8	1.7	88.1	2.2	88.5	2.0
42	79.9	2.2	89.1	2.1	90.0	1.7	80.1	1.2	87.9	2.5	89.1	2.1
44	80.1	2.0	88.3	2.1	89.1	1.3	80.1	1.5	88.5	1.5	88.0	2.0
46	79.5	1.5	88.4	2.2	89.6	1.1	79.8	1.5	89.2	1.7	88.9	1.8
48	80.8	2.0	88.4	1.4	88.7	2.0	80.0	2.6	88.9	1.8	89.3	1.3
50	81.5	1.9	88.6	1.6	90.0	1.5	81.3	1.7	89.2	1.4	88.7	1.5

Approximately 10% of increment has obtained by training ANN's individually (Figure 4.7). For each subject, ANN trained 10 times and then mean accuracy and the standard deviation is calculated and the maximum accuracy rate of 96% was obtained when ANN was trained individually (Table 4.8). In the performance plot of individualized ANNs for subject 1 and subject 2, the best validation performance is 0.0255 at 11 epoch and 0.217 at epoch 15 respectively (Figure 4.8 & Figure 4.9).



Training Function: Scaled Conjugate Gradient, Levenberg-Marquardt and Bayesian Regression

Input: 5 feature x 2 channel

Figure 4.7 Structure of individualized ANN training with SCG, LM and BR functions for the feature set 1

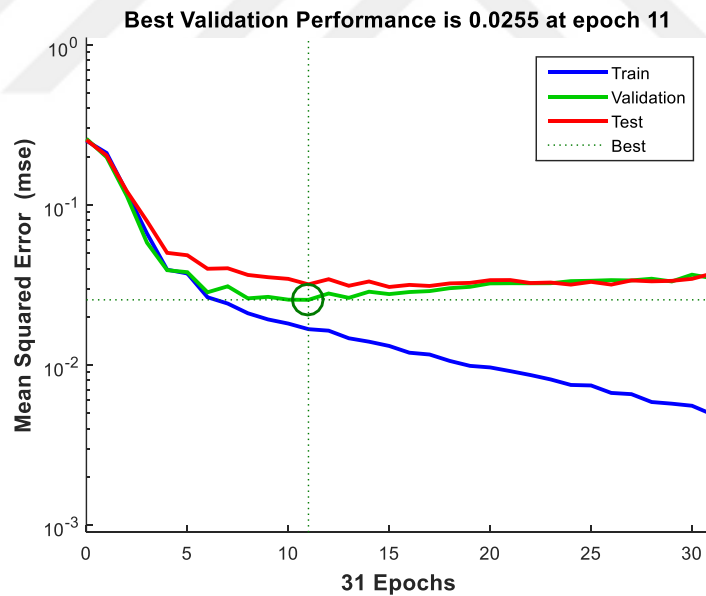


Figure 4.8 Performance plot of individualized ANN training for subject 1

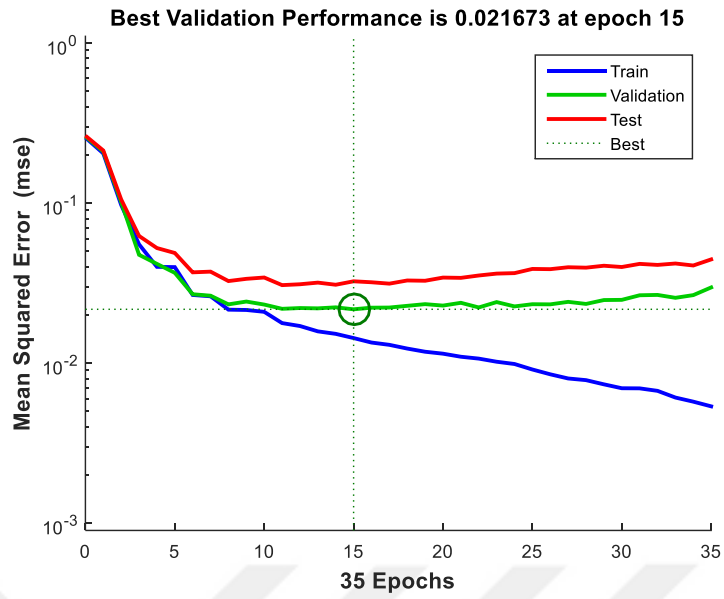


Figure 4.9 Performance plot of individualized ANN training for subject 2

Table 4.8 Accuracy rate of individually trained ANNs.

HLN	Set 1 - SCG	Set 1 - SCG	Set 1 - LM	Set 1 - LM	Set 2 - BR	Set 2 - BR
	Mean	±Std	Mean	±Std	Mean	±Std
2	85.9	6.0	91.3	1.3	91.3	0.8
4	92.3	1.1	95.0	0.7	94.6	0.6
6	92.2	1.0	94.8	0.6	94.4	1.1
8	92.9	1.0	95.3	0.7	95.2	0.5
10	93.0	1.1	95.5	0.6	95.0	1.2
12	93.3	1.2	95.1	0.9	95.7	0.8
14	92.5	1.0	95.5	0.8	95.3	0.8
16	93.1	1.2	95.5	0.6	95.6	0.8
18	93.7	0.9	95.3	0.7	95.7	0.7
20	93.3	1.1	95.4	0.5	95.6	1.0
22	93.3	0.6	95.3	0.6	95.5	0.8
24	93.4	0.8	94.5	1.3	95.8	0.8
26	93.1	1.2	95.3	0.2	95.3	0.5
28	92.9	1.0	95.6	0.8	95.6	0.7
30	92.7	1.3	95.8	0.6	95.5	0.9
32	93.7	1.1	95.7	0.6	95.4	1.0
34	93.6	1.7	95.9	0.7	95.5	0.8
36	93.8	1.3	95.7	0.7	95.2	0.8
38	92.8	1.1	95.5	0.4	95.2	1.1
40	93.2	1.5	95.7	0.6	95.2	0.8
42	93.4	1.3	95.7	0.7	95.7	0.7
44	93.3	1.2	95.6	0.9	95.4	0.6
46	93.5	1.3	95.7	0.8	95.5	0.5
48	92.9	1.2	95.8	0.4	95.4	0.6
50	92.9	1.4	96.0	1.0	95.5	0.7

An external data set is acquired from Musab Salih Sakar. Two ANN's trained with LM function and 40 HLN's (Figure 4.10). As a result of the training process, 89.08% accuracy and 87.98% accuracy are obtained for feature set 1 and feature set 2 respectively (Table 4.9). Best validation performances were calculated as 0.062447 at epoch 10 for feature set 1 (Figure 4.11) and 0.062428 at epoch 8 for the feature set 2 (Figure 3.12).

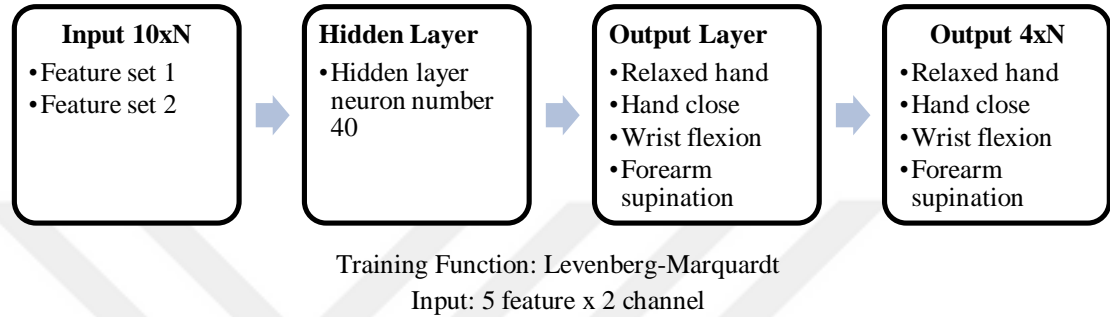


Figure 4.10 Structure of individualized ANN training with LM function for the feature set 1

Table 4.9 Accuracy rate of trained ANNs with external data.

Feature Set	Mean Accuracy %	± Std
Feature Set 1	89.08	2.10
Feature Set 2	87.98	6.91

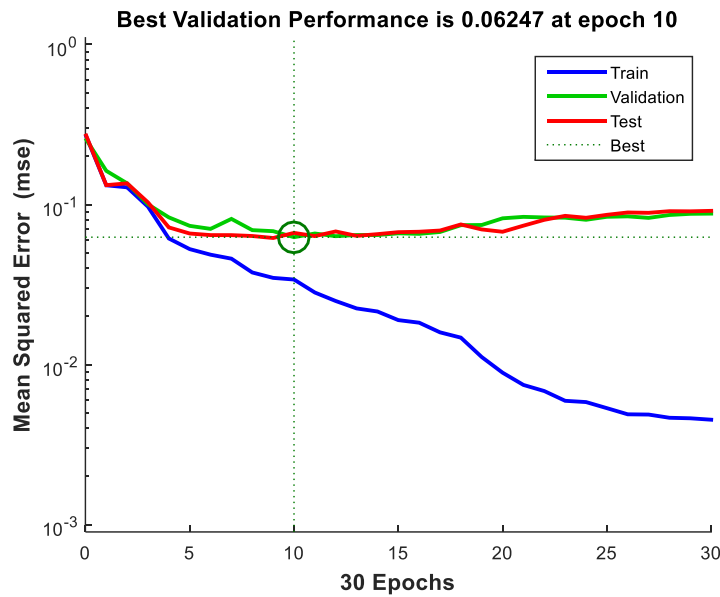


Figure 4.11 Performance plot of trained ANN with the feature set 1

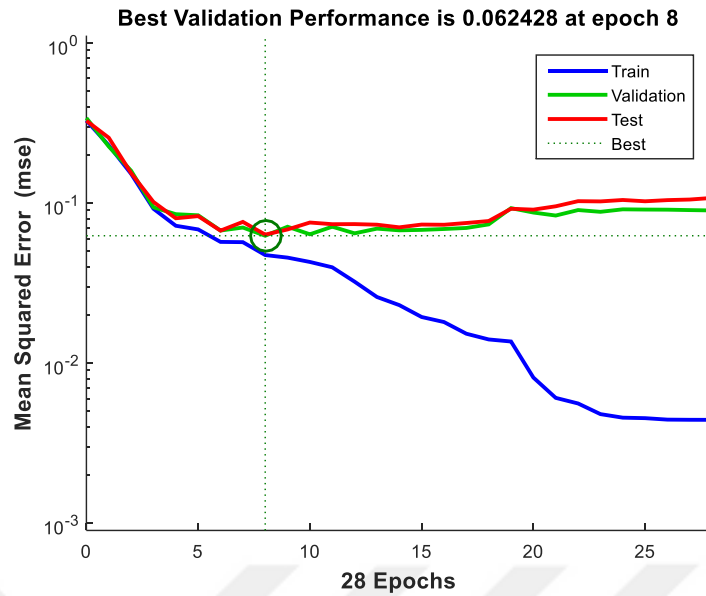
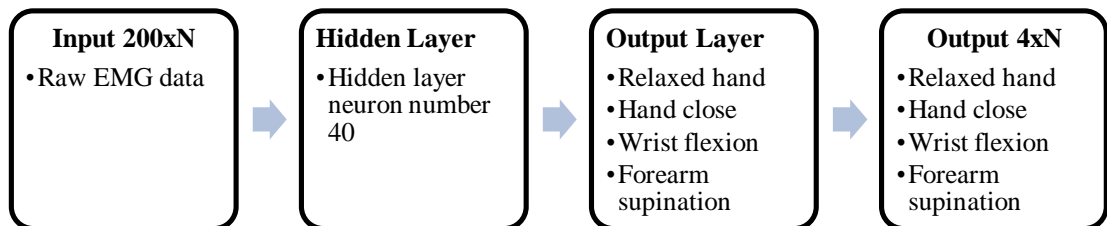


Figure 4.12 Performance plot of trained ANN with the feature set 2

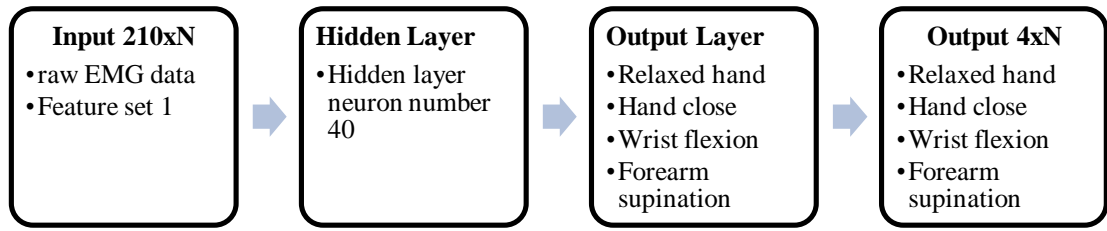
Two ANN's trained with LM function and 40 HLN's by using only raw EMG data and raw EMG data with the addition of the feature set 1 (Figure 4.13 & Figure 4.14). As a result of the training process, 84.42% accuracy and 93.25% accuracy are obtained for raw data and raw data with the addition of the feature set 1, respectively. Best validation performances were calculated as 0.15008 at epoch 14 for raw data and 0.044472 at epoch 7 for raw data with the addition of the feature set 1.



Training Function: Levenberg-Marquardt

Input: 100 raw data sample x 2 channel

Figure 4.13 Structure of individualized ANN training with LM function for raw EMG data



Training Function: Levenberg-Marquardt

Input: (100 raw EMG data sample + 5 feature) x 2 channel

Figure 4.14 Structure of individualized ANN training with LM function for the feature set 1 and raw EMG data

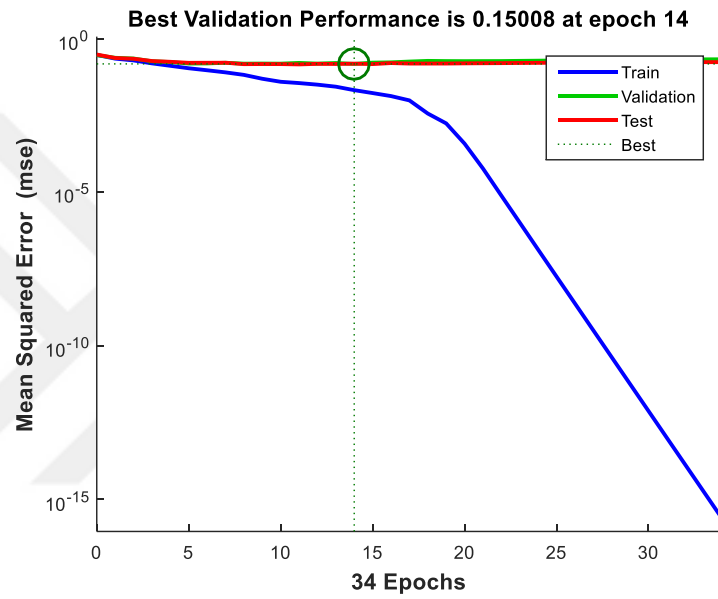


Figure 4.15 Performance plot of trained ANN with raw EMG data

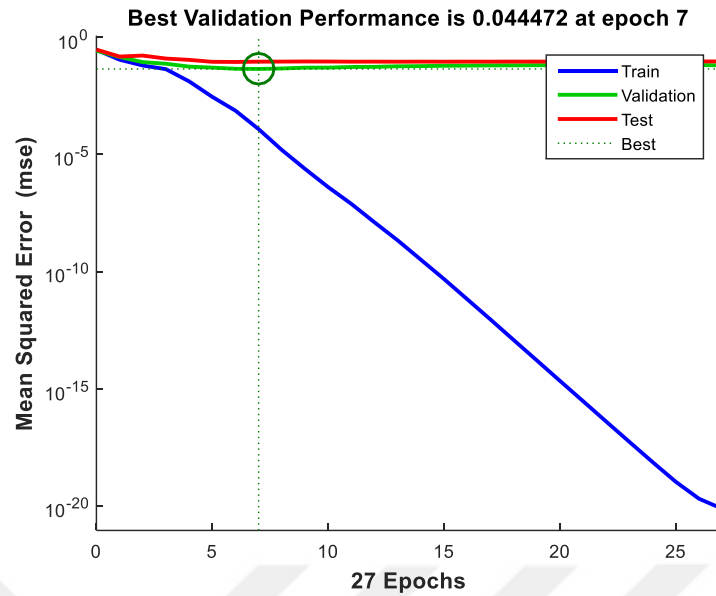


Figure 4.16 Performance plot of trained ANN with raw EMG data and feature set 1

4.1.4 Effects of Feature Groups on ANN Accuracy

In order to determine the effect of feature groups on ANN accuracy, the groups were excluded one by one. Feature group 3 gave the lowest accuracy rate with 59.26%. In contrast, Feature group 1 gave the highest accuracy rate of 84.20% individually. When the groups were removed one by one, the most significant decrease was seen when group 1 was removed with approximately 7% (Table 4.10).

Table 4.10 Effects of feature groups on ANN accuracy

Input Feature Groups	Accuracy %	\pm Std
Feature Group 1+2+3	90.01	1.2
Feature Group 1+2	89.31	0.89
Feature Group 1+3	87.55	1.11
Feature Group 2+3	82.19	1.57
Feature Group 1	84.20	1.03
Feature Group 2	78.31	1.68
Feature Group 3	59.26	0.75

ANN has been trained by removing features one by one. When MAV, VAR, WL, DASDV, and WAMP features excluded individually, the accuracy rate of the

classifier has been increased slightly (Table 4.11). Even On the other hand, when the RMS, MFL, and SSC were excluded, the mean accuracy rates decreased. This contradicts some points with the experiment of the individual testing of the features in Section 3.5. For example, although MAV is the feature that provides the highest accuracy for the EI group, accuracy is increased when excluded alone. On the other hand, although the SSC feature remained below the average for individual classification success, overall classification success decreased when excluded. This showed that the success of individual classification of properties can be misleading.

Table 4.11 Effect of feature exclusion on ANN accuracy

Excluded Feature	Accuracy %	\pm Std
MAV	91.13	1.46
RMS	88.76	1.79
LOG	90.13	1.79
SSI	90.86	2.01
VAR	91.00	2.58
MFL	89.65	1.36
WL	91.12	1.24
AAC	90.67	0.73
DASDV	91.28	1.06
SSC	88.61	1.96
WAMP	91.17	1.36

Hardware has been installed for signal acquisition. After collecting data with hardware, features were extracted from this data. In the trials; The effect of feature groups, individual features, and generalization and individualization approaches on classification performance was evaluated. The best results were obtained between 30 and 50 hidden layer neurons. In addition, it was observed that the individualization of the classifier improves performance. When the frequency information feature group was excluded, there was no significant change in performance. When SCG was used as a training function, it was observed that performance was lower than LM and BR training functions.

CHAPTER FIVE

CONCLUSION

In this thesis, it is aimed to classify the transradial EMG signals obtained from a 2 channel EMG sensor using an ANN. Myoware TM Muscle Sensor (AT-04-001) was used in order to receive the EMG signal. Arduino Mini Pro Leonardo and HC-06 Bluetooth Communication device are used to transmit the signals received from a two-channel EMG sensor to the computer.

Time-domain features were used in the classification of hand and wrist movements. A maximum success rate of 90% with a generalization approach. However, a maximum accuracy rate of 95% was obtained when ANN was trained individually.

EMG data obtained from ten subjects were used for hand and wrist movements. When the classification of the four movements was examined, when SCG is used as a training function, accuracy, sensitivity, specificity and precision metrics are significantly decreased. On the other hand, there was no significant difference between LM and BR training in terms of used performance metrics. When the number of hidden layer neurons was selected between 30 and 50, ANNs gave the best results. However, increasing the number of hidden layer neurons increases the training time.

An external EMG data set is obtained and used for further ANN training trials. In these trials, feature set 1, feature set 2, raw EMG data and raw EMG data with the feature set 1 addition used as input vectors. Accuracy rates calculated as 89.08%, 87.98%, 84.42% and 93.25% respectively. The addition of the feature set 1 to raw data, increased the overall accuracy rating by approximately 8%.

All studies were conducted using ten subjects and this affects the objectivity of success rates. In order to successfully classify more movements, EMG signals can be acquired, processed and used for neural network training with more than two sensors. In addition, the scope of further studies can be expanded by obtaining data from more subjects to ensure that the results are more accurate.

In this study, all movements investigated individually, however in further studies combinations of movements such as forearm supination of a closed hand, should be investigated. Furthermore, proportional movements are not included in this study. In future studies, proportional movements should be investigated. With a successful classification of proportional and combined movements, the classifier may be implemented on a prosthetic arm prototype. Although the signals received from the lower arm are classified in this study, the basic principle can be studied for any other limb in the body.



REFERENCES

- Al-Ani, A., Koprinska, I., Naik, G. R., & Khushaba, R. N. (2016). A dynamic channel selection algorithm for the classification of EEG and EMG data. *Proceedings of the International Joint Conference on Neural Networks, October*, 4076–4081.
- Arduino. (n.d.). *What is Arduino?* Retrieved January 9, 2020, from <https://www.arduino.cc/en/Guide/Introduction>
- Arduino, S. (2018). *Arduino Leonardo with Headers*. Retrieved January 9, 2020, from Arduino website: <https://store.arduino.cc/usa/leonardo>
- Arjunan, S. P., & Kumar, D. K. (2010). Decoding subtle forearm flexions using fractal features of surface electromyogram from single and multiple sensors. *Journal of NeuroEngineering and Rehabilitation*, 7(53), 1–26.
- Caesarendra, W. (2018). Classification method of hand gestures based on support vector machine. *Computer Engineering and Applications Journal*, 7(3), 179–190
- Chowdhury, R. H., Reaz, M. B. I., Bin Mohd Ali, M. A., Bakar, A. A. A., Chellappan, K., & Chang, T. G. (2013). Surface electromyography signal processing and classification techniques. *Sensors (Switzerland)*, 13(9), 12431–12466.
- Currie, C., Nistler, A. R., Port, G., Downey, C., McDonald, D., Sabatino, J., & Souto, S. (2017). *Design and development of a myoelectric transradial prosthesis*. Retrieved May 29, 2019, from https://web.wpi.edu/Pubs/E-project/Available/E-project-042717-103143/unrestricted/HandMQP_FinalReport.pdf
- Dopico, P. J. (2016). *A subject specific surface electromyography model for estimating l4/l5 compressive loading*. Master Thesis, University of Tennessee Health Science Center, Memphis, TN.
- Englehart, K., Hudgins, B., Parker, P. A., & Stevenson, M. (1999). Classification of the myoelectric signal using time-frequency based representations. *Medical Engineering and Physics*, 21(6–7), 431–438.

- Farina, D., & Aszmann, O. (2014). Bionic limbs: clinical reality and academic promises. *Science Translational Medicine*, 6(257), 12.
- Frontera, W. R., & Ochala, J. (2015). Skeletal muscle: a brief review of structure and function. *Behavior Genetics*, 96(3), 183–195.
- Geethanjali, P. (2016). Myoelectric control of prosthetic hands: state-of-the-art review. *Medical Devices: Evidence and Research*, 9, 247–255.
- Hadley, G. (2007). Essential clinical anatomy. *Journal of Anatomy*, 211(3), 413
- Hargrove, L. J., Englehart, K., & Hudgins, B. (2007). A comparison of surface and intramuscular myoelectric signal classification. *IEEE Transactions on Biomedical Engineering*, 54(5), 847–853.
- Hudgins, B., Parker, P., & Scott, R. N. (1993). A new strategy for multifunction myoelectric control. *IEEE Transactions on Biomedical Engineering*, 40(1), 82–94.
- Iqbal, N. V., Subramaniam, K., & Shaniba Asmi, P. (2018). A Review on Upper-Limb Myoelectric Prosthetic Control. *IETE Journal of Research*, 64(6), 740–752.
- Jenkins, D. B. (2009). *Hollinshead's functional anatomy of the limbs and back* (9th ed.). Saunders: Elsevier Health Sciences.
- Jiang, N., Vest-Nielsen, J. L., Muceli, S., & Farina, D. (2012). EMG-based simultaneous and proportional estimation of wrist/hand kinematics in uni-lateral trans-radial amputees. *Journal of Neuroengineering and Rehabilitation*, 9(1), 42.
- Joochim, C., & Siriwatcharakul, N. (2019). Artificial human arm controlled by muscle electromyography (EMG). *ESIT 2018 - 3rd International Conference on Engineering Science and Innovative Technology*, 1–5.
- Chung, K., & Chung, H. (2008). *Gross Anatomy*. Philadelphia: Lippincott Williams & Wilkins.
- Khushaba, R. N., Al-Timemy, A. H., Al-Ani, A., & Al-Jumaily, A. (2017). A framework of temporal-spatial descriptors-based feature extraction for improved

- myoelectric pattern recognition. *IEEE Transactions on Neural Systems and Rehabilitation Engineering*, 25(10), 1821–1831.
- Kung, T. A., Bueno, R. A., Alkhalefah, G. K., Langhals, N. B., Urbanchek, M. G., & Cederna, P. S. (2013). Innovations in prosthetic interfaces for the upper extremity. *Plastic and Reconstructive Surgery*, 132(6), 1515–1523.
- Luksch, T. (2010). *Human-like control of dynamically walking bipedal robots. Optimization*. Retrieved from <https://agrosy.informatik.uni-kl.de/fileadmin/Literatur/Luksch10.pdf>
- Marchessault, J. A., McKay, P. L., & Hammert, W. C. (2011). Management of upper limb amputations. *Journal of Hand Surgery*, 36(10), 1718–1726.
- Meier, R. H. (2004). *Functional Restoration of Adults and Children with Upper Extremity Amputation*, New York: Demos Medical.
- Micera, S., Carpaneto, J., & Raspopovic, S. (2010). Control of hand prostheses using peripheral information. *IEEE Reviews in Biomedical Engineering*, 3, 48–68.
- Moore, K. L., Dalley, A. F., & Agur, A. M. R. (2013). *Clinically oriented anatomy*. Philadelphia: Lippincott Williams & Wilkins.
- Oweis, R. J., Rihani, R., & Alkhawaja, A. (2014). ANN-based EMG classification for myoelectric control. *International Journal of Medical Engineering and Informatics*, 6(4), 365–380.
- Phinyomark, A., Hirunviriyaya, S., Limsakul, C., & Phukpattaranont, P. (2010). Evaluation of EMG feature extraction for hand movement recognition based on euclidean distance and standard deviation. *ECTI-CON 2010 - The 2010 ECTI International Conference on Electrical Engineering/Electronics, Computer, Telecommunications and Information Technology*, 856–860.
- Phinyomark, A., Phukpattaranont, P., & Limsakul, C. (2012). Feature reduction and selection for EMG signal classification. *Expert Systems with Applications*, 39(8), 7420–7431.

- Phukan, N., Kakoty, N. M., Shivam, P., & Gan, J. Q. (2019). Finger movements recognition using minimally redundant features of wavelet denoised EMG. *Health and Technology*, 9(4), 579–593.
- Reaz, M. B. I., Hussain, M. S., & Mohd-Yasin, F. (2006). Techniques of EMG signal analysis: detection, processing, classification and applications. *Biological Procedures Online*, 8(1), 11–35.
- Saladin, K. S. (2010). *Anatomy & physiology: the unity of form and function (6th ed.)*. New York: McGraw-Hill.
- Smith, L. H., Kuiken, T. A., & Hargrove, L. J. (2015). Use of probabilistic weights to enhance linear regression myoelectric control. *Journal of Neural Engineering*, 12(6), 066030.
- Sparkfun. (2015). *3-lead Muscle / Electromyography Sensor for Microcontroller Applications*. Retrieved September 13, 2019, from www.AdvancerTechnologies.com
- Sparkfun. (2019). *MyoWare Muscle Sensor - SEN-13723 - SparkFun Electronics*. Retrieved September 13, 2019, from <https://www.sparkfun.com/products/13723>
- Stanos, S. P., & Rivers, W. E. (2014). Physical medicine and rehabilitation. *Encyclopedia of the Neurological Sciences* (2nd ed.) (897–901). San Diego: Academic Press.
- Tengku Zawawi, T. N. S., Abdullah, A. R., Jopri, M. H., Sutikno, T., Saad, N. M., & Sudirman, R. (2018). A review of electromyography signal analysis techniques for musculoskeletal disorders. *Indonesian Journal of Electrical Engineering and Computer Science*, 11(3), 1136–1146.
- Tkach, D., Huang, H., & Kuiken, T. A. (2010). Study of stability of time-domain features for electromyographic pattern recognition. *Journal of NeuroEngineering and Rehabilitation*, 7(1), 21.
- Yu, S., Jeong, E., Hong, K., & Lee, S. (2012). Classification of nine directions using the maximum likelihood estimation based on electromyogram of both forearms.

Biomedical Engineering Letters, 2(2), 129–137.

Zardoshti-Kermani, M., Wheeler, B. C., Badie, K., & Hashemi, R. M. (1995). EMG feature evaluation for movement control of upper extremity prostheses. *IEEE Transactions on Rehabilitation Engineering*, 3(4), 324–333.

